ACS chemical biology

pubs.acs.org/acschemicalbiology

Articles

Halogenation-Dependent Effects of the Chlorosulfolipids of *Ochromonas danica* on Lipid Bilayers

Frank R. Moss III, Gabrielle E. Cabrera, Grace M. McKenna, Giulio J. Salerno, Steven R. Shuken, Matthew L. Landry, Thomas M. Weiss, Noah Z. Burns,* and Steven G. Boxer*

Cite This: *ACS Chem. Biol.* 2020, 15, 2986–2995

Read Online

ACCESS | Metrics & More | Article Recommendations | Supporting Information

ABSTRACT: The chlorosulfolipids are amphiphilic natural products with stereochemically complex patterns of chlorination and sulfation. Despite their role in toxic shellfish poisoning, potential pharmacological activities, and unknown biological roles, they remain understudied due to the difficulties in purifying them from natural sources. The structure of these molecules, with a charged sulfate group in the middle of the hydrophobic chain, appears incompatible with the conventional lipid bilayer structure. Questions about chlorosulfolipids remain unanswered partly due to the unavailability of structural analogues with which to conduct structure–function studies. We approach this problem by combining enantioselective total synthesis and membrane biophysics. Using a combination of Langmuir pressure–area isotherms of lipid monolayers, fluorescence imaging of vesicles, mass spectrometry imaging, natural product isolation, small-angle X-ray scattering, and cryogenic electron microscopy, we show that danicalipin A (**1**) likely inserts into lipid bilayers in the headgroup region and alters their structure and phase behavior. Specifically, danicalipin A (**1**) thins the bilayer and fluidizes it, allowing even saturated lipid to form fluid bilayers. Lipid monolayers show similar fluidizing upon insertion of danicalipin A (**1**). Furthermore, we show that the halogenation of the molecule is critical for its membrane activity, likely due to sterically controlled conformational changes. Synthetic unchlorinated and monochlorinated analogues do not thin and fluidize lipid bilayers to the same extent as the natural product. Overall, this study sheds light on how amphiphilic small molecules interact with lipid bilayers and the importance of stereochemistry and halogenation for this interaction.

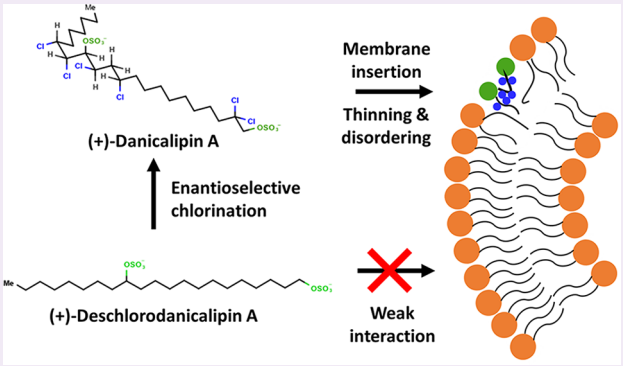

The stereochemically complex chlorosulfolipids of the freshwater microalga *Ochromonas danica* were first described by Haines et al. and Elovson and Vagelos in 1969.[1−3] These amphiphilic molecules are characterized by an unusually high level of chlorination and sulfation. The chlorosulfolipids danicalipin A, malhamensilipin A, and mytilipin A are all cytotoxic and include some of the causative agents of toxic shellfish poisoning.[4,5] Malhamensilipin A is also a protein tyrosine kinase inhibitor.[6] The major chlorosulfolipid in *O. danica* is danicalipin A, which has six chlorines and two sulfates, all with defined stereochemistry on a linear 22-carbon chain (see Figure 1).[7,8] Danicalipin A's biological function in *O. danica*, the mechanism of human toxicity, and potential pharmacological utility remain poorly studied due to the difficulty of purifying it from natural sources. Danicalipin A has remained a popular synthetic target for chemists due to its complexity and the need for pure material for biological studies.[9−11] Danicalipin A was initially assumed to be a purely defensive molecule, but subsequent studies indicated that it may also have functions in *O. danica*. *O. danica* produces few other identified lipids besides danicalipin A and its precursors, and they may make up the majority of the polar lipid content of the flagellar membrane, suggesting a functional role.[12] While their toxic effects are well documented, it remains unclear how *O. danica* avoids self-toxicity from the chlorosulfolipids they produce and whether chlorosulfolipids form an integral part of their membranes. Biophysicists have puzzled over how this unconventional structure, with a charged sulfate moiety in the middle of the hydrophobic region, could form part of biological membranes or otherwise interact with membranes.[13] While hypothetical structures of bilayers composed of chlorosulfolipids have been proposed, there have been no experiments probing the structure or physical properties of membranes composed partly or entirely of chlorosulfolipids. Understanding how this molecule forms and interacts with membranes would broaden our understanding of how

Received: July 31, 2020
Accepted: October 1, 2020
Published: October 9, 2020

https://dx.doi.org/10.1021/acschembio.0c00624
ACS Chem. Biol. 2020, 15, 2986–2995

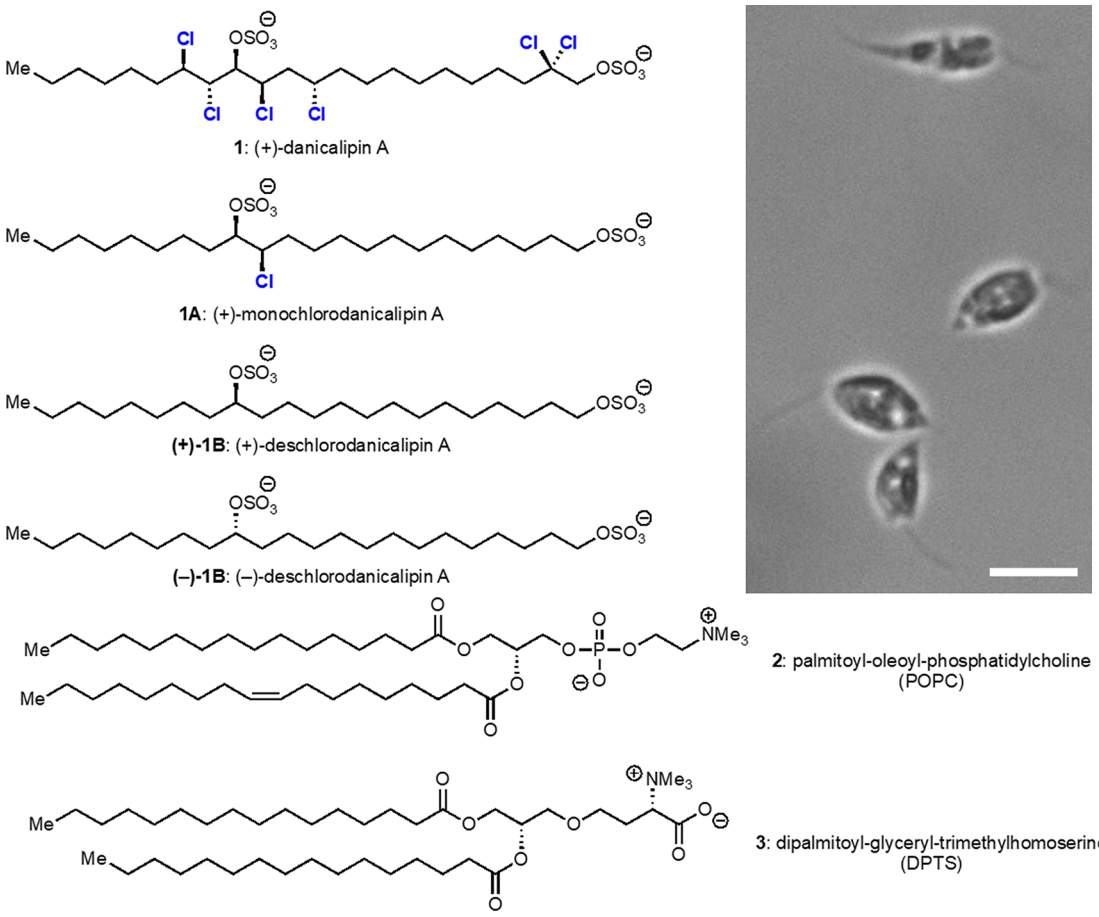

Figure 1. Structures of danicalipin A (**1**), its presumed biosynthetic precursors **1A**, (+)-**1B**, (−)-**1B**, as well as POPC (**2**) and DPTS (**3**). Note the charged sulfate group in the middle of the hydrophobic chain of danicalipin A (**1**), making it incompatible with the conventional lipid bilayer structure. *O. danica* cells are shown in the upper right. Scale bar, 10 μm.

amphiphilic small molecules, like sterols and many small-molecule drugs, interact with membranes.

It is not well understood what the effects of the chlorination pattern and stereochemistry are on the toxicity or potential biological functions of danicalipin A (**1**). To answer these questions, we have combined enantioselective chemical synthesis and membrane biophysics. We show that danicalipin A (**1**) does not form lipid bilayers on its own but readily incorporates into bilayers composed of conventional mammalian and algal lipids. We have produced (+)-danicalipin A (**1**) by modifying our previous synthetic route to (−)-danicalipin A, along with three analogues to enlarge structure−function relationships. Langmuir monolayer analysis, small-angle X-ray scattering (SAXS), and fluorescence microscopy of lipid mixtures containing danicalipin A (**1**) reveal that danicalipin A (**1**) fluidizes lipid bilayers when it inserts into them, likely due to its position at the membrane−water interface. Furthermore, we use the synthetic unchlorinated analogue and a monochlorinated analogue (Figure 1) to show that the halogenation pattern affects danicalipin A (**1**)'s membrane activity. We also directly show that chlorosulfolipids and other halosulfolipids are located in *O. danica*'s cellular membranes with imaging mass spectrometry and mass spectrometry-based lipidomics.

METHODS

Detailed synthetic and experimental methods are available in the Supporting Information.

RESULTS AND DISCUSSION

Halogen Incorporation and Distribution of Halosulfolipids. Although the chlorosulfolipids were first described over 50 years ago, much is unexplored about the subcellular distribution of danicalipin A (**1**) in *O. danica*, its biosynthesis, and its functions. We first examined the halogen selectivity of the biosynthesis of halosulfolipids and their distribution in *O. danica* cells to determine the chemical diversity of halosulfolipids that the biosynthetic enzymes make and their localization. Additionally, the halosulfolipids produced under different growth conditions may provide information about their function. Previously, Haines et al. briefly reported that *O. danica* will grow in synthetically defined media with either bromide or iodide as the sole halide source and that bromo- and possibly iodosulfolipids are produced under these conditions.[14] Recently, Vanderwal et al. reported that *O. danica* does indeed produce bromosulfolipids, including the fully brominated analogue of danicalipin A with the corresponding stereo- and regiochemistry.[15] However, no data have been presented to support the claim that *O. danica* may also be able to produce iodosulfolipids, which may be unstable due to the weak C−I bonds. We attempted to grow *O. danica* in a rich medium and synthetically defined media with

https://dx.doi.org/10.1021/acschembio.0c00624
ACS Chem. Biol. 2020, 15, 2986−2995

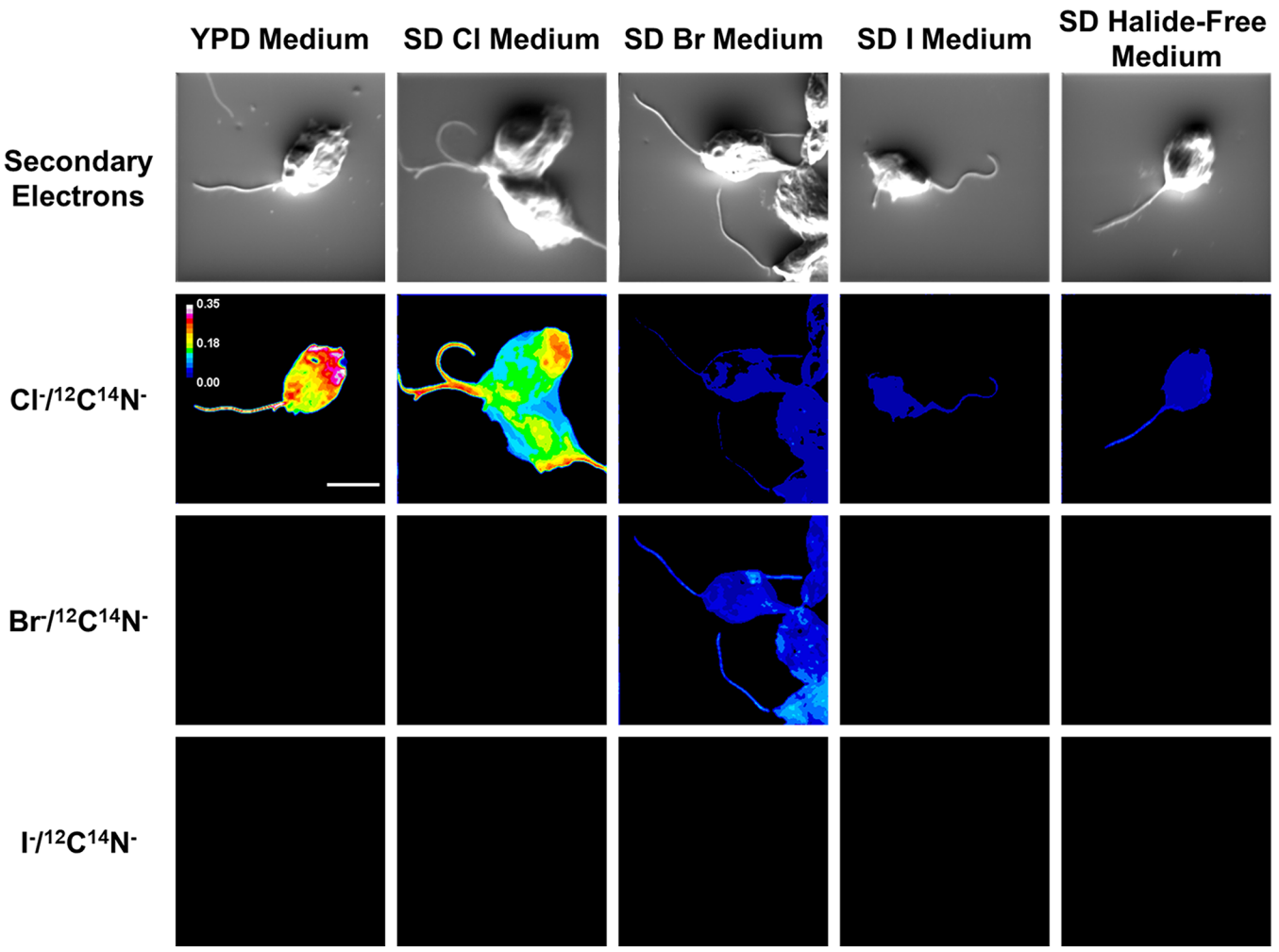

Figure 2. Ion ratio images and secondary electron images of cells grown in different media. Images are corrected for isotopic abundance of halides. The same threshold values were applied to each image to make quantitative comparisons. All images have the halide signal from the substrate subtracted for clarity. Scale bar, 5 μm.

the ammonium salts of chloride, bromide, and iodide as the sole halide sources. Additionally, we attempted to grow the alga in a synthetically defined medium with no added halide source. We note that chloride contamination is pervasive, and despite using components with high chemical purity and low halide contamination, some halide contamination, particularly chloride, is inevitable. The algae grew in all of the media but at a slower rate and to lower cell densities in the synthetically defined media, and they grew especially slowly in the synthetically defined medium with iodide and the medium without added halides (see Figure S2e). This result indicates that chloride, and possibly the chlorosulfolipids, is important to the normal growth and function of *O. danica*.[1]

We next used nanoscale secondary ion mass spectrometry (NanoSIMS) imaging and LC-MS to determine whether cells can utilize each halide and what halosulfolipids are produced under each condition.[16,17] Cells from each medium were fixed, rinsed with water, and dried on oxidized silicon substrates for NanoSIMS analysis. The cells were rinsed so that any free halides in the cells and media would be washed away, leaving only halogenated molecules that are embedded in membranes or tightly bound to proteins. The cells grown in iodide minimal media support this assumption as no iodide remains in the cells after fixation (Figure 2). Since the primary ion beam fragments the sample to monatomic and small polyatomic ions, it is not possible to know from which molecules the halide secondary ions arise, but we presume that halosulfolipids are the only halogenated natural products of *O. danica*.

With NanoSIMS, we quantified the amount of Cl^-, Br^-, and I^- in the cells grown in each medium and normalized each quantity to CN^- to account for differences in ion yield and topography. As expected, the cells grown in rich medium and chloride-defined medium contained mainly chloride in their halogenated molecules, with only a small amount of bromide and virtually no iodide (Figure 2 and Table S1). After extensively washing the cells with water, they still contain a large amount of chloride, indicating that the chlorinated molecules are likely stably inserted into the membranes of the fixed cells. Interestingly, we see no evidence for chlorosulfolipid enrichment in the flagellum relative to the cell body, as was previously reported.[12] The previous study suggesting flagellar enrichment was performed with lipid extraction and 2D TLC analysis, which may have not identified some of the lipid species, particularly the exotic lipids found in *O. danica*. NanoSIMS is a direct method for quantification of lipid concentration *in situ* in membranes and does not involve lipid extraction, so danicalipin A (**1**) is likely not enriched in the flagellar membrane. Organelle purification and lipidomic

https://dx.doi.org/10.1021/acschembio.0c00624
ACS Chem. Biol. 2020, 15, 2986−2995

analysis, as well as NanoSIMS analysis of thin sections of cells, may reveal enrichment of danicalipin A (**1**) in some cellular compartments (see Section S6 for further discussion of subcellular distribution of chlorosulfolipids). When the medium contains bromide as the only added halide, the bromide content of the cells increases by 350-fold relative to the chloride-defined medium, consistent with the biosynthesis of bromosulfolipids. Despite our best efforts to exclude chloride from this medium, there is still significant chloride contamination with Cl^-/Br^- equal to 0.3 (see Table S1 for quantitative analysis). However, when the cells were grown in medium with iodide as the only added halide, only a small increase in iodide incorporation into the cells was observed (2-fold increase relative to the chloride-defined medium). This observation implies that, unlike bromide, iodide cannot substitute for chloride in halosulfolipid biosynthesis. It is not clear from this experiment whether the as yet unknown halogenase in *O. danica* does not accept iodide as a halogen source or whether iodosulfolipids are formed but rapidly dehalogenate. Finally, in the halide-defined medium with no added halide, the halide content of the cells was decreased to 13% of the halide content of cells grown in the chloride-defined medium. This represents the amount of halide contamination in the salts used to make the media. It is notable that the cells still grow in this medium, but it is not clear whether they make a smaller amount of halosulfolipids or the same quantity of less halogenated halosulfolipids. To answer these questions, we extracted the halosulfolipids from *O. danica* grown in each medium and analyzed them with LC-MS.

The results of the LC-MS analysis of the sulfolipid composition of *O. danica* cells grown under various conditions are shown in Figure S2. As expected, the major sulfolipid in cells grown in rich YPD medium is danicalipin A (**1**), the fully hexachlorinated natural product. When the cells are grown in chloride-defined medium containing 9.4 mM chloride (lower than the chloride concentration in YPD), danicalipin A (**1**) is still a major sulfolipid, but the penta-, tetra-, and trichlorosulfolipid precursors of danicalipin A are also abundant. When the cells are grown in bromide-defined medium, the fully brominated danicalipin A analogue is observed. Additionally, mixed bromo-/chlorosulfolipids and a wide variety of bromosulfolipids bearing fewer than six bromides are present. This is consistent with the results of the NanoSIMS experiments, which showed that bromide was incorporated into *O. danica* cells when they were grown in bromide-defined medium, but that they also incorporated chloride from trace contamination. Finally, when the cells are grown in iodide-defined medium, no iodosulfolipids are observed. Instead, chlorosulfolipids with zero to six chlorides are present. This observation is also consistent with the NanoSIMS data, which showed that cells did not incorporate iodide when grown in iodide-defined medium, but that they did incorporate trace chloride contamination. It appears that *O. danica* cells synthesize sulfolipids bearing fewer chlorine atoms as the chloride concentration in the medium decreases. However, even at the very low levels of chloride that result from trace contaminants in the salts used to make the media, they still make highly chlorinated molecules. We never observed the fully unchlorinated analogue of danicalipin A (deschlorodanicalipin A, (+)-**1B**) as a major natural product. These results, along with the slow growth rates and lower final cell densities of *O. danica* in the media without added chloride, further reinforce the hypothesis that danicalipin A (**1**) biosynthesis is vital to the growth of the cells and serves a biological purpose other than solely as a defensive secondary metabolite for *O. danica*. However, we cannot currently separate chlorosulfolipid biosynthesis from other biological functions of chloride because there are no genetic tools for *O. danica*, and biosynthetic enzymes have not been identified.

Biophysical Analysis of Lipid Monolayers. With evidence that chlorosulfolipids are indeed part of the membranes of *O. danica* cells, we next performed a battery of biophysical experiments to determine how chlorosulfolipids interact with membranes, how they change the physical properties of membranes, and how they alter the structure of membranes. We utilized the model membrane systems of lipid bilayers and lipid monolayers composed of the common phospholipid 1-palmitoyl-2-oleoyl-glycero-3-phosphocholine (POPC, **2**) and 1,2-dipalmitoyl-*sn*-glycero-3-*O*-4′-(*N*,*N*,*N*-trimethyl)-homoserine (DPTS, **3**), a representative of a relatively rare class of glycerolipid that is found in *O. danica* and is thought to be a substitute for phosphatidylcholine lipids in some algae.[18−20]

In order to examine the importance of halogenation for the membrane activity of halosulfolipids, we completed an enantioselective synthesis of an analogue of danicalipin A with no chlorines, which we refer to as deschlorodanicalipin A ((−)-**1B**) (see Figure 1). We examined the effect of the stereochemistry of the sulfate at C14 by synthesizing the other enantiomer of (−)-**1B**, (+)-**1B**. Both analogues interacted with lipid monolayers and lipid bilayers in the same manner (see Section S13), so we performed further experiments with only (−)-**1B**. We also synthesized a monochlorinated danicalipin A analogue, referred to as monochlorodanicalipin A (**1A**), with a single chlorine on C13, one of the positions that may be key to controlling the solution conformation of danicalipin A (**1**) (see Figure 1).[21] Both of these molecules are thought to be biosynthetic precursors to danicalipin A (**1**), and small amounts of them are found in *O. danica* cells; however, they cannot be isolated from algae in sufficient quantities or purity for biophysical analysis. It was previously shown by Carreira et al. that changing the stereochemistry and number of chlorines on danicalipin A (**1**) changes its solution conformation and biological activity.[9,21,22] We reasoned that analogues with fewer chlorines would also have altered solution conformations and that these conformational changes might alter the interactions of the molecules with membranes.

We first determined whether danicalipin A (**1**), monochlorodanicalipin A (**1A**), and deschlorodanicalipin A ((−)-**1B**) would spontaneously insert into lipid monolayers at the air−water interface. Insertion into monolayers can be monitored with a Langmuir trough because the mean molecular area (MMA), which is recorded with a Wilhelmy plate, will increase if molecules insert into the monolayer.[23] We recorded the pressure−area isotherms for DPTS (**3**), 1:1 DPTS (**3**):danicalipin A (**1**), 1:1 DPTS (**3**):monochlorodanicalipin A (**1A**), and 1:1 DPTS (**3**):deschlorodanicalipin A ((−)-**1B**) (see Figure 3). We attempted to form a monolayer of pure danicalipin A (**1**), but all attempts resulted in no increase in surface pressure, suggesting that it disperses into the water subphase rather than staying at the air−water interface. The isotherm for DPTS (**3**) appears similar to the isotherm for DPPC (1,2-dipalmitoyl-*sn*-glycero-3-phosphocholine), except that it is shifted to higher MMAs. It displays a phase transition at approximately 5 mN/m like DPPC,

https://dx.doi.org/10.1021/acschembio.0c00624
ACS Chem. Biol. 2020, 15, 2986−2995

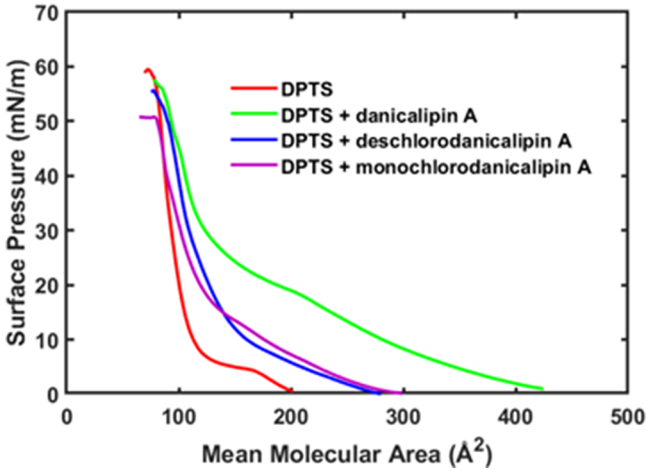

Figure 3. Incorporation of danicalipin A (**1**), monochlorodanicalipin A (**1A**), and deschlorodanicalipin A ((−)-**1B**) into monolayers of DPTS (**3**). Pressure−area isotherms of DPTS (**3**) (red), 1:1 DPTS (**3**):danicalipin A (**1**) (green), 1:1 DPTS (**3**):monochlorodanicalipin A (**1A**) (purple), and 1:1 DPTS (**3**):deschlorodanicalipin A ((−)-**1B**) (blue). Danicalipin A (**1**) perturbs the DPTS (**3**) isotherm to a greater extent than monochlorodanicalipin A (**1A**) or deschlorodanicalipin A ((−)-**1B**). MMAs are calculated from the amount of DPTS (**3**) added.

consistent with its transition temperature being close to that of DPPC. The transition temperatures for the palmitoyl and stearoyl analogues of DPTS have been reported to be 53 and 59 °C, very close to the transition temperatures of PSPC and DSPC.[24] These data indicate that the unique trimethylhomoserine headgroup of DPTS (**3**) increases its MMA in monolayers versus DPPC, but the dipalmitoyl chains result in similar phase behavior. Interestingly, when danicalipin A (**1**) is included in the lipid mixture used to form the monolayer, the isotherm shifts to significantly higher MMAs, and the shape of the isotherm changes. This shows that danicalipin A (**1**) forms part of the monolayer rather than being dispersed in the subphase. The phase transition also shifts to higher surface pressure. This effect is usually observed when increasing the temperature of the monolayer, not adding another component. On the other hand, when monochlorodanicalipin A (**1A**) and deschlorodanicalipin A ((−)-**1B**) are included in the lipid mixture used to form the monolayer, the resulting isotherm is only slightly shifted to higher MMAs. For (−)-**1B**, the phase transition does not shift to higher surface pressure, and for **1A**, the phase transition shifts to only slightly higher surface pressure. This result implies that the deschloro- and monochloro-analogues, which only differ from danicalipin A (**1**) in their halogenation, do not interact with DPTS (**3**) monolayers as strongly as danicalipin A (**1**).

We further explored the interaction of danicalipin A and its descholoro- and monochloro-analogues with DPTS (**3**) by

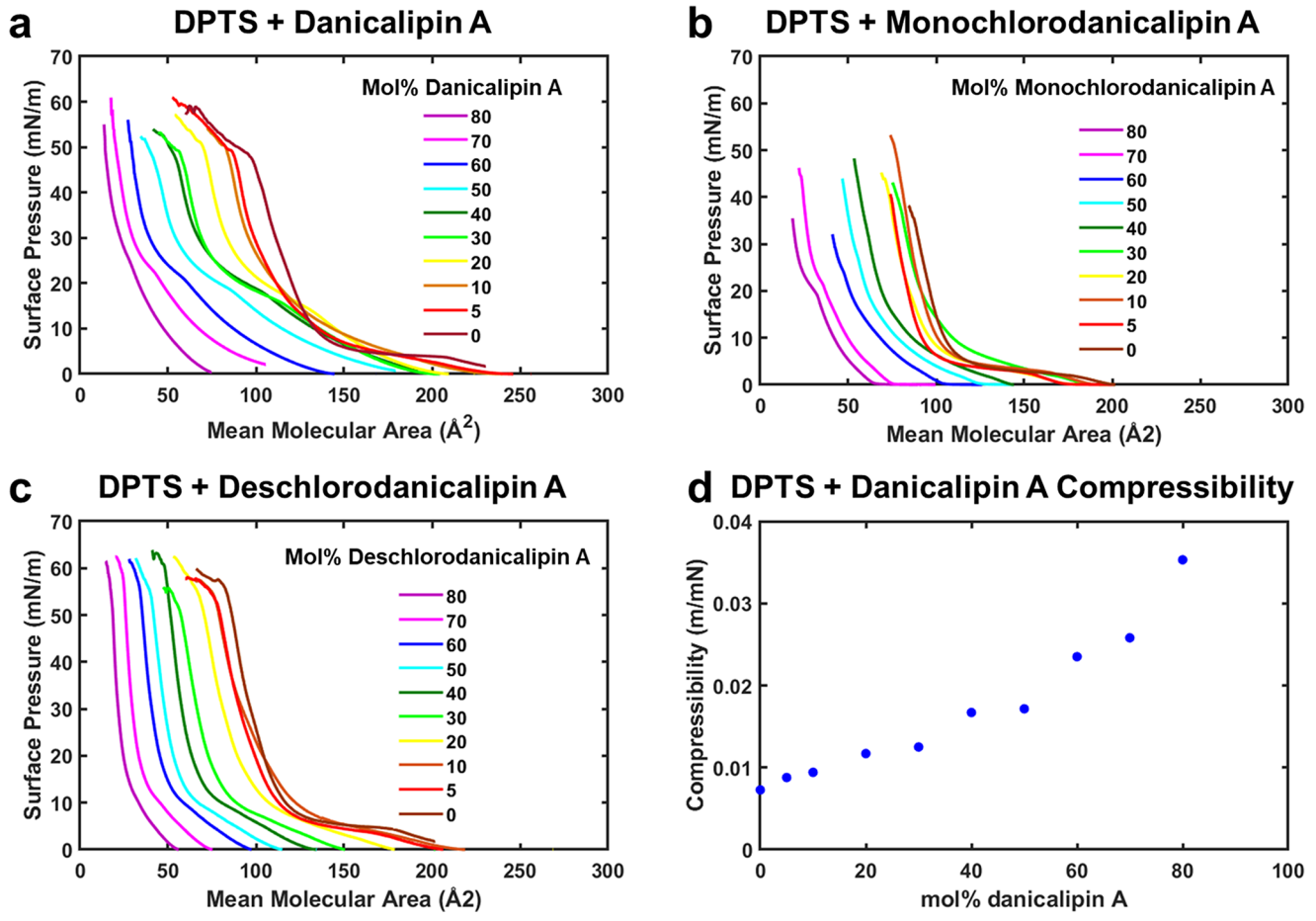

Figure 4. Pressure−area isotherms and compressibilities of mixtures of danicalipin A (**1**), deschlorodanicalipin A ((−)-**1B**), and monochlorodanicalipin A (**1A**) and DPTS (**3**). DPTS (**3**) makes up the rest of the mol % of the mixture for the indicated sulfolipid mol %.

https://dx.doi.org/10.1021/acschembio.0c00624
ACS Chem. Biol. 2020, 15, 2986−2995

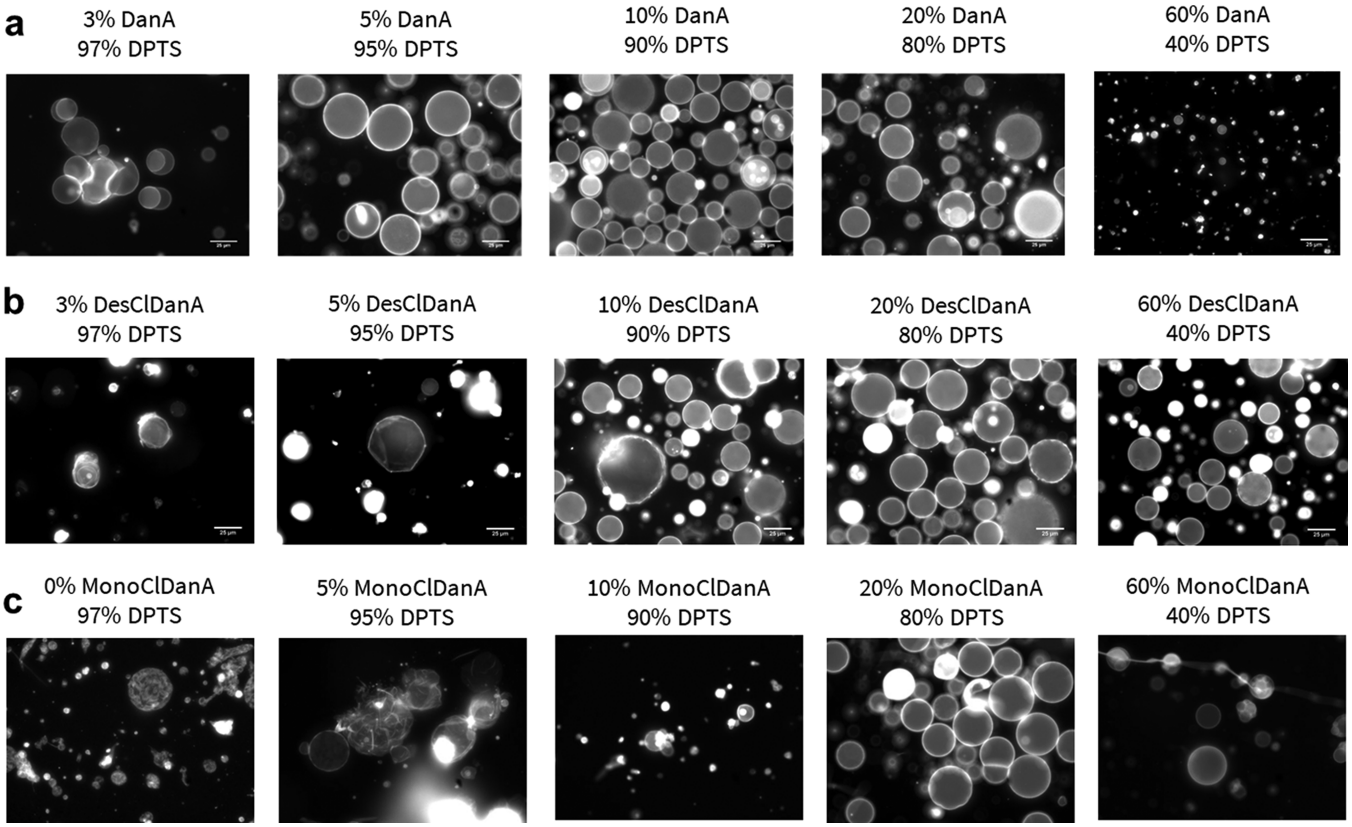

Figure 5. Micrographs of GUVs containing sulfolipids. Incorporation of (a) danicalipin A (**1**), (b) deschlorodanicalipin A ((−)-**1B**), and (c) monochlorodanicalipin A (**1A**) into GUVs of DPTS (**3**) and their influence on DPTS (**3**) phase behavior. DanA = danicalipin A (**1**), DesClDanA = deschlorodanicalipin A ((−)-**1B**), MonoClDanA = monochlorodanicalipin A (**1A**). Scale bar, 25 μm.

varying the ratio of DPTS (**3**) to sulfolipid. We kept the total number of moles of lipid constant and changed the molar ratio of DPTS (**3**) to sulfolipid. The resulting pressure−area isotherms are shown in Figure 4. The phase transition in the isotherms with danicalipin A shifts to higher surface pressure until the mol % of danicalipin A (**1**) reaches approximately 40%. As danicalipin A (**1**) occupies a smaller molecular volume than DPTS (**3**), the isotherms also shift to progressively lower MMAs as more danicalipin A (**1**) is added. In contrast, as the mol % of deschlorodanicalipin A ((−)-**1B**) increases, the isotherms simply shift to lower MMAs, and the slope of the phase transition increases without shifting to higher surface pressure. This is consistent with the isotherms in Figure 3 that suggested that deschlorodanicalipin A ((−)-**1B**) does not interact with DPTS (**3**) monolayers in the same manner as **1**. Monochlorodanicalipin A (**1A**) displays a behavior intermediate between danicalipin A (**1**) and deschlorodanicalipin A ((−)-**1B**) as it shifts the phase transition to somewhat higher surface pressures (Figure 4c). However, the phase transition also seems to disappear as it did with deschlorodanicalipin A ((−)-**1B**). This result indicates that the chlorine in the C13 position can partially rescue the ability of danicalipin A (**1**) to insert into lipid bilayers. The behavior of the sulfolipids and DPTS (**3**) stands in stark contrast of that of mixtures of phospholipids with single chain amphiphiles like cholesterol and fatty acids (see Section S10).

Finally, we measured the compressibility of the danicalipin A (**1**) and DPTS (**3**) mixtures from the pressure−area isotherms at 32 mN/m, which approximates the lipid packing in a bilayer. The compressibility of the monolayer increases as the percentage of danicalipin A (**1**) in the mixture increases, indicating that the danicalipin A (**1**) is fluidizing and disordering the DPTS (**3**). This stands in contrast to cholesterol, which causes an increase and then a decrease in the compressibility of monolayers of DPPC as it undergoes phase changes (see Section S10 and Figure S9).

Biophysical Analysis of Lipid Bilayers. With the knowledge that danicalipin A (**1**) and deschlorodanicalipin A ((−)-**1B**) insert into monolayers, we next evaluated whether these molecules would insert into lipid bilayers. We attempted to form giant unilamellar vesicles (GUVs) via gentle hydration of lipid films containing 20:80 mol % sulfolipid:POPC (**2**) and a wide range of sulfolipid:DPTS (**3**) ratios (40 μM total lipid, 1.2−24 μM sulfolipid). POPC (**2**) GUVs were observed when 20 mol % danicalipin A (**1**) was added to the lipid mixture, indicating that danicalipin does not simply destroy lipid bilayers but has more subtle effects on their structure (Figure 5a, also see Section S8). GUVs made from a mixture of 20 mol % danicalipin A (**1**) in POPC (**2**) appeared uniform when visualized with Texas Red DHPE (TR). DPTS (**3**) GUVs cooled to room temperature (RT) appeared as nonspherical gel-phase aggregates, as expected for a lipid with a transition temperature above RT. Strikingly, when just 4−5 mol % of danicalipin A (**1**) is included in the lipid mixture with DPTS (**3**), the resulting GUVs appeared round and fluid at RT (see Section S8 for a further discussion of GUV morphology and phase behavior). GUVs were observed for up to 50−60 mol % danicalipin A (**1**). This observation demonstrates that danicalipin A (**1**) interacts with and changes the phase behavior of lipid bilayers.

https://dx.doi.org/10.1021/acschembio.0c00624
ACS Chem. Biol. 2020, 15, 2986−2995

We repeated GUV formation experiments with DPTS (**3**) and deschlorodanicalipin A ((−)-**1B**) to evaluate how it interacts with lipid bilayers. Consistent with the monolayer experiments, deschlorodanicalipin A ((−)-**1B**) did not induce the formation of fluid GUVs until a significantly higher mol % (10−15%) (Figure 5b). Unlike with danicalipin A (**1**), at 60 mol % deschlorodanicalipin A ((−)-**1B**), it was possible to form many large GUVs. Finally, monochlorodanicalipin A (**1A**) displayed similar behavior, with an onset of GUV formation between 10−15 mol % and an upper limit of 60 mol % (Figure 5c).

Next, we attempted to determine how danicalipin A (**1**) interacts with lipid bilayers by performing SAXS on small unilamellar vesicles (SUVs) composed of POPC (**2**) and danicalipin A (**1**).[23] We chose POPC (**2**) because it is fluid at RT, so the scattering behavior of mixtures of POPC (**2**) and danicalipin A (**1**) or deschlorodanicalipin A ((−)-**1B**) could be directly compared to pure POPC (**2**). The scattering data were used to build a model of the excess electron density of the lipid bilayer of an SUV by fitting the SAXS scattering curve. We then observed changes in the excess electron density profiles between POPC (**2**) and POPC (**2**)/danicalipin A (**1**) and POPC (**2**)/deschlorodanicalipin A ((−)-**1B**) SUVs in order to see how danicalipin A (**1**) and deschlorodanicalipin A ((−)-**1B**) alter the structure of the bilayer and where in the bilayer they reside.[23,25] We performed SAXS on 50 nm POPC (**2**) SUVs with 0, 10, and 30 mol % of both danicalipin A (**1**) and deschlorodanicalipin A ((−)-**1B**) (4 mM total lipid, 0.4−1.2 mM sulfolipid) (Figure 6a). It is clear from the electron

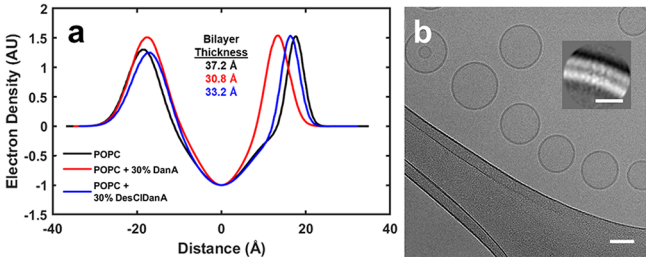

Figure 6. Structure of bilayers containing danicalipin A (**1**). (a) Electron density profiles from fitting of small-angle X-ray scattering of POPC (**2**) SUVs containing 30% of either danicalipin A (**1**) or deschlorodanicalipin A ((−)-**1B**) show that danicalipin A (**1**) thins POPC (**2**) bilayers. (b) Cryo-EM image of SUVs composed of POPC (**2**) and 30% danicalipin A (**1**) and 2D class average of bilayer segments (inset) demonstrate unilamellarity of SUVs. Scale bar, 50 nm. Scale bar inset, 5 nm.

density curves in Figure 6a that both danicalipin A (**1**) and deschlorodanicalipin A ((−)-**1B**) alter the POPC (**2**) bilayer structure. Comparing the electron density curves for SUVs with danicalipin A (**1**) or deschlorodanicalipin A ((−)-**1B**), both molecules thin the bilayer, with 30 mol % danicalipin A (**1**) thinning the POPC (**2**) bilayer by almost 20% (see Section S12). At both 10 and 30 mol %, danicalipin A (**1**) thins the bilayer more than the unchlorinated analogue. The outer leaflet of the bilayer (to the right of the hydrophobic trough) is preferentially thinned. This observation is consistent with insertion of sulfolipids at the bilayer interface, which would be stabilized by positive curvature. Additionally, both sulfolipids widen the distributions of electron density at the headgroup regions. This widening of electron density likely results from the sulfolipids inserting at the surface of the bilayer and reducing lipid order. This observation is consistent with the previous GUV formation experiments showing that danicalipin A (**1**) induces DPTS (**3**) to form fluid bilayers at RT. Consistent with the monolayer experiments, danicalipin A (**1**) appears to have a greater effect on the bilayer structure than deschlorodanicalipin A ((−)-**1B**) does. The SAXS data clearly show that both halosulfolipids insert into POPC (**2**) bilayers and alter their structure, but the two sulfolipids alter the POPC (**2**) structure to different extents and/or have different membrane affinities.

As fitting of SAXS data is inherently dependent on the model used, we also sought to directly confirm these results of bilayer thinning with cryogenic electron microscopy (cryo-EM). Cryo-EM images of SUVs composed of POPC (**2**) and danicalipin A (**1**) confirmed that they had a bilayer structure (Figure 6b and Figures S8 and S9). Furthermore, 2D classification and averaging of bilayer segments confirmed membrane thinning upon incorporation of danicalipin A (**1**) (Section S9). This membrane thinning, which stands in contrast to the membrane thickening observed when cholesterol is added to POPC (**2**),[26,27] strongly suggests that danicalipin A (**1**) inserts into the bilayer at the hydrophilic interface and does not fully insert into the hydrocarbon region.

Model for Interaction of Danicalipin A with Lipid Bilayers. As depicted in our working model in Figure 7,

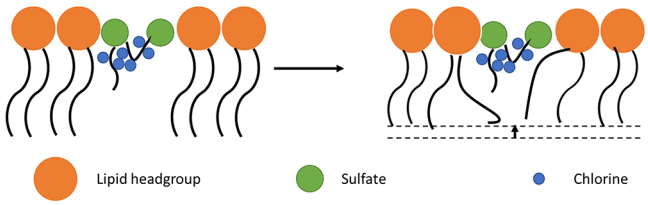

Figure 7. Model for the interaction of danicalipin A (**1**) with lipid bilayers. Danicalipin A (**1**) inserts at the hydrophobic/hydrophilic interface so that the sulfates are hydrated while the hydrophobic moieties are buried in the hydrophobic region of the bilayer. The gauche interactions between vicinal chlorines, which are determined by the stereochemistry of the carbon−chlorine bonds, favor this conformation. The lipid tails distort to fill the space under the danicalipin A (**1**), disordering and thinning the bilayer.

insertion at the bilayer interface causes the surface area of the bilayer to increase, leaving a packing defect beneath the danicalipin A (**1**) molecule. The bilayer stress created by this void is relieved by disordering of acyl chains from neighboring lipids, causing the membrane to thin to conserve molecular volumes. The same membrane thinning effect has been observed for melatonin, which also inserts at the surface of the bilayer.[28,29] Full insertion into the bilayer, as in the case of sterols, generally causes the membrane to thicken as no void is created by the sterol, and acyl chains tend to become more ordered. This model is consistent with the GUV formation and Langmuir trough experiments that both show a disordering of lipids upon addition of danicalipin A (**1**).

CONCLUSIONS

We have shown that, despite its exotic structure, danicalipin A (**1**) inserts into and forms part of the structure of lipid bilayers. Furthermore, it fluidizes the fully saturated algal lipid DPTS (**3**) and causes it to form fluid GUVs at RT. We hypothesize that danicalipin A (**1**) partially inserts at the surface of monolayers and bilayers so that its sulfate groups remain

https://dx.doi.org/10.1021/acschembio.0c00624
ACS Chem. Biol. 2020, 15, 2986−2995

hydrated, while the hydrophobic regions of danicalipin A (**1**) dip into the hydrocarbon region of the bilayer. This partial insertion causes the lipid tails to reorganize to fill the space left unoccupied by the danicalipin A (**1**) and prevents tight packing of DPTS (**3**) into the gel phase.

Halogenation of the alkyl chain had a large effect on the membrane activity of sulfolipids tested. Removing the chlorines from danicalipin A (**1**) to form deschlorodanicalipin A ((−)-**1B** and (+)-**1B**) greatly reduces its membrane activity. It has been hypothesized that the bulky, electronegative chlorines cause the molecule to adopt certain preferred conformations due to gauche interactions. Inverting stereochemistry of the chlorinated carbons and reducing the degree of chlorination on danicalipin A (**1**) change its preferred solution configuration in various solvents and hydrophobic cages.[21,22,30] We hypothesize that a similar mechanism occurs in aqueous solutions and lipid bilayers. The chlorination pattern might alter the conformational landscape to favor conformations that interact with membranes more strongly and cause danicalipin A (**1**) to partition more strongly into bilayers. When the chlorines are not present, membrane-interacting conformations are higher energy and not significantly populated, and the unhalogenated molecules have lower affinities for lipid bilayers. This *in vitro* result is consistent with *in vivo* data showing that deschlorodanicalipin A ((+)-**1B**) is an order of magnitude less toxic to brine shrimp than danicalipin A (**1**).[9]

We also investigated whether there are any functional differences for substitutionally distinct sulfolipids *in vivo* in *O. danica* by growing cells in synthetically defined media with the various halides or no added halide. *O. danica* grew very slowly in medium with low chloride concentration and did not achieve the same cell densities as in the higher chloride media. We then confirmed that iodosulfolipids are not produced in the medium with only iodide added. However, bromine appears to be able to functionally substitute for chlorine in halosulfolipids. The slower growth rates in media with lower halide concentrations suggest that halosulfolipids do in fact play a functional role in *O. danica*, and they are not solely toxic defensive molecules. Alternatively, chloride may be required for other functions in *O. danica*. As the danicalipin A biosynthetic enzymes have not been identified, we cannot specifically inhibit chlorosulfolipid biosynthesis to rule out this possibility.

Single-chain amphiphiles, such as cholesterol and hopanoids, play a critical role in the structure and function of biological membranes.[31,32] It has been hypothesized that single-chain amphiphiles may have formed the membranes of early life forms rather than the more complex double-chain lipids found in modern membranes.[33−36] While specific conditions under which fatty acids will assemble into vesicles have been found, there remain many questions about how single chain amphiphiles could form functional membranes. In this work, we have shown that the single chain amphiphile danicalipin A (**1**) can integrate into lipid bilayers when mixed with bilayer-forming lipids and that it may have an important structural role in the membranes of *O. danica*. Relatively simple modifications like halogenation and stereochemical scrambling have large effects on this role. Early chemical modification of single chain amphiphiles by primordial organisms might have created an array of molecules for forming membranes with different properties. Additionally, bioactive amphiphilic small molecules like melatonin, serotonin, long-chain alcohols, anesthetics, and benzodiazepines have been shown to interact with membranes.[28,37] These interactions control bioavailability, off-target effects, and membrane protein activities via changes in membrane structure. This study has revealed halogenation as an important determining factor in controlling the mode of membrane interaction of danicalipin A (**1**), and this mechanism may be useful for designing membranes with beneficial properties and membrane-altering molecules. Future studies will further elucidate the biological functions of danicalipin A (**1**) by exploration of subcellular localization via organelle purification and genetic studies to find the enzymes responsible for halogenation.

■ ASSOCIATED CONTENT

Supporting Information

The Supporting Information is available free of charge at https://pubs.acs.org/doi/10.1021/acschembio.0c00624.

Synthetic schemes, synthetic and experimental methods, supplementary data, and supplementary discussion (PDF)

■ AUTHOR INFORMATION

Corresponding Authors

Noah Z. Burns − *Department of Chemistry, Stanford University, Stanford, California 94305, United States;* orcid.org/0000-0003-1064-4507; Email: nburns@stanford.edu

Steven G. Boxer − *Department of Chemistry, Stanford University, Stanford, California 94305, United States;* orcid.org/0000-0001-9167-4286; Email: sboxer@stanford.edu

Authors

Frank R. Moss III − *Department of Chemistry, Stanford University, Stanford, California 94305, United States;* orcid.org/0000-0002-6149-6447

Gabrielle E. Cabrera − *Department of Chemistry, Stanford University, Stanford, California 94305, United States*

Grace M. McKenna − *Department of Chemistry, Stanford University, Stanford, California 94305, United States*

Giulio J. Salerno − *Department of Chemistry, Stanford University, Stanford, California 94305, United States*

Steven R. Shuken − *Department of Chemistry, Stanford University, Stanford, California 94305, United States*

Matthew L. Landry − *Department of Chemistry, Stanford University, Stanford, California 94305, United States*

Thomas M. Weiss − *Stanford Synchrotron Radiation Laboratory, Stanford Linear Accelerator Center, Stanford University, Menlo Park, California 94025, United States*

Complete contact information is available at: https://pubs.acs.org/10.1021/acschembio.0c00624

Notes

The authors declare no competing financial interest.

■ ACKNOWLEDGMENTS

This work was supported by Stanford University, the Terman foundation, the National Institutes of Health (GM118044 to S.G.B.), the NSF Biophysics Program (to S.G.B.), the National Science Foundation (graduate fellowship to S.R.S.), and the Center for Molecular Analysis and Design (graduate fellowships to F.R.M. and G.M.M.). Use of the Stanford Synchrotron Radiation Lightsource, SLAC National Accelerator Laboratory,

is supported by the U.S. Department of Energy, Office of Science, Office of Basic Energy Sciences under Contract DE-AC02-76SF00515. The SSRL Structural Molecular Biology Program is supported by the DOE Office of Biological and Environmental Research, and by the National Institutes of Health, National Institute of General Medical Sciences (including P41GM103393). The contents of this publication are solely the responsibility of the authors and do not necessarily represent the official views of NIGMS or NIH. The Pilatus detector at BL4-2 was funded under National Institutes of Health Grant S10OD021512. Part of this work was performed at the Stanford Nano Shared Facilities (SNSF), supported by the NSF under award ECCS-1542152. The Cameca NanoSIMS 50L at the Stanford Nano Shared Facilities is supported by the National Science Foundation (Award 0922648). We thank C. Hitzman of the Stanford Nano Shared Facilities for assistance with the NanoSIMS 50L. Mass spectrometry was performed at the Vincent Coates Foundation Mass Spectrometry Laboratory, Stanford University. We thank R. Jinkerson for assistance with culturing *O. danica*. Cryo-EM was performed at the Stanford-SLAC CryoEM Facility. We thank E. Montabana for assistance with EM sample preparation and data collection. Sputter coating was performed at the Cell Sciences Imaging Facility at Stanford University. We thank P. Chu and D. Wu at the Stanford University Animal Histology Services for assistance with cryosectioning.

REFERENCES

(1) Elovson, J., and Vagelos, P. R. (1969) A New Class of Lipids: Chlorosulfolipids. *Proc. Natl. Acad. Sci. U. S. A. 62*, 957−963.
(2) Mayers, G. L., Pousada, M., and Haines, T. H. (1969) Microbial sulfolipids. III. The disulfate of (+)-1,14-docosanediol in Ochromonas danica. *Biochemistry 8*, 2981−2986.
(3) Haines, T. H., Pousada, M., Stern, B., and Mayers, G. L. (1969) Microbial Sulpholipids: (*R*)-13-Chloro-1-(*R*)-14-docosanediol Disulphate and Polychlorosulpholipids in Ochromonas danica. *Biochem. J. 113*, 565−566.
(4) Ciminiello, P., Dell'Aversano, C., Fattorusso, E., Forino, M., Magno, S., Di Rosa, M., Ianaro, A., and Poletti, R. (2002) Structure and stereochemistry of a new cytotoxic polychlorinated sulfolipid from Adriatic shellfish. *J. Am. Chem. Soc. 124*, 13114−13120.
(5) Ciminiello, P., Fattorusso, E., Forino, M., Di Rosa, M., Ianaro, A., and Poletti, R. (2001) Structural elucidation of a new cytotoxin isolated from mussels of the Adriatic sea. *J. Org. Chem. 66*, 578−582.
(6) Chen, J. L., Proteau, P. J., Roberts, M. A., Gerwick, W. H., Slate, D. L., and Lee, R. H. (1994) Structure of Malhamensilipin A, an Inhibitor of Protein Tyrosine Kinase, from the Cultured Chrysophyte *Poterioochromonas malhamensis*. *J. Nat. Prod. 57*, 524−527.
(7) Bedke, D. K., Shibuya, G. M., Pereira, A., Gerwick, W. H., Haines, T. H., and Vanderwal, C. D. (2009) Relative stereochemistry determination and synthesis of the major chlorosulfolipid from Ochromonas danica. *J. Am. Chem. Soc. 131*, 7570−7572.
(8) Kawahara, T., Kumaki, Y., Kamada, T., Ishii, T., and Okino, T. (2009) Absolute configuration of chlorosulfolipids from the chrysophyta Ochromonas danica. *J. Org. Chem. 74*, 6016−6024.
(9) Bailey, A. M., Wolfrum, S., and Carreira, E. M. (2016) Biological Investigations of (+)-Danicalipin A Enabled Through Synthesis. *Angew. Chem., Int. Ed. 55*, 639−643.
(10) Landry, M. L., Hu, D. X., McKenna, G. M., and Burns, N. Z. (2016) Catalytic Enantioselective Dihalogenation and the Selective Synthesis of (−)-Deschloromytilipin A and (−)-Danicalipin A. *J. Am. Chem. Soc. 138*, 5150−5158.
(11) Bedke, D. K., and Vanderwal, C. D. (2011) Chlorosulfolipids: Structure, synthesis, and biological relevance. *Nat. Prod. Rep. 28*, 15−25.
(12) Chen, L. L., Pousada, M., and Haines, T. H. (1976) The flagellar membrane of Ochromonas danica. Lipid composition. *J. Biol. Chem. 251*, 1835−1842.
(13) Mayers, G. L., and Haines, T. H. (1967) A microbial sulfolipid. II: Structural studies. *Biochemistry 6*, 1665−1671.
(14) Haines, T. H. (1973) Halogen- and sulfur-containing lipids of Ochromonas. *Annu. Rev. Microbiol. 27*, 403−411.
(15) White, A. R., Duggan, B. M., Tsai, S. C., and Vanderwal, C. D. (2016) The Alga Ochromonas danica Produces Bromosulfolipids. *Org. Lett. 18*, 1124−1127.
(16) Moss, F. R., and Boxer, S. G. (2016) Atomic Recombination in Dynamic Secondary Ion Mass Spectrometry Probes Distance in Lipid Assemblies: A Nanometer Chemical Ruler. *J. Am. Chem. Soc. 138*, 16737−16744.
(17) Frisz, J. F., Lou, K., Klitzing, H. A., Hanafin, W. P., Lizunov, V., Wilson, R. L., Carpenter, K. J., Kim, R., Hutcheon, I. D., Zimmerberg, J., Weber, P. K., and Kraft, M. L. (2013) Direct chemical evidence for sphingolipid domains in the plasma membranes of fibroblasts. *Proc. Natl. Acad. Sci. U. S. A. 110*, 613−622.
(18) Brown, A. E., and Elovson, J. (1974) Isolation and characterization of a novel lipid, 1(3),2-diacylglyceryl-(3)-O-4′-(N, N, N-trimethyl)homoserine, from Ochromonas danica. *Biochemistry 13*, 3476−3482.
(19) Riekhof, W. R., Naik, S., Bertrand, H., Benning, C., and Voelker, D. R. (2014) Phosphate starvation in fungi induces the replacement of phosphatidylcholine with the phosphorus-free betaine lipid diacylglyceryl-*N, N, N*-trimethylhomoserine. *Eukaryotic Cell 13*, 749−757.
(20) Rozentsvet, O. A., Dembitsky, V. M., and Saksonov, S. V. (2000) Occurrence of diacylglyceryltrimethylhomoserines and major phospholipids in some plants. *Phytochemistry 54*, 401−407.
(21) Fischer, S., Huwyler, N., Wolfrum, S., and Carreira, E. M. (2016) Synthesis and Biological Evaluation of Bromo- and Fluorodanicalipin A. *Angew. Chem., Int. Ed. 55*, 2555−2558.
(22) Boshkow, J., Fischer, S., Bailey, A. M., Wolfrum, S., and Carreira, E. M. (2017) Stereochemistry and biological activity of chlorinated lipids: a study of danicalipin A and selected diastereomers. *Chem. Sci. 8*, 6904−6910.
(23) Moss, F. R., III, Shuken, S. R., Mercer, J. A. M., Cohen, C. M., Weiss, T. M., Boxer, S. G., and Burns, N. Z. (2018) Ladderane phospholipids form a densely packed membrane with normal hydrazine and anomalously low proton/hydroxide permeability. *Proc. Natl. Acad. Sci. U. S. A. 115*, 9098−9103.
(24) Sato, N., and Murata, N. (1991) Transition of lipid phase in aqueous dispersions of diacylglyceryltrimethylhomoserine. *Biochim. Biophys. Acta, Lipids Lipid Metab. 1082*, 108−111.
(25) Narayanan, T., Weerakkody, D., Karabadzhak, A. G., Anderson, M., Andreev, O. A., and Reshetnyak, Y. K. (2016) pHLIP Peptide Interaction with a Membrane Monitored by SAXS. *J. Phys. Chem. B 120*, 11484−11491.
(26) Olsen, B. N., et al. (2013) The structural basis of cholesterol accessibility in membranes. *Biophys. J. 105*, 1838−1847.
(27) Leftin, A., et al. (2014) Area per lipid and cholesterol interactions in membranes from separated local-field (13)C NMR spectroscopy. *Biophys. J. 107*, 2274−2286.
(28) Drolle, et al. (2013) Effect of melatonin and cholesterol on the structure of DOPC and DPPC membranes. *Biochim. Biophys. Acta, Biomembr. 1828*, 2247−2254.
(29) Choi, Y., et al. (2014) Melatonin directly interacts with cholesterol and alleviates cholesterol effects in dipalmitoylphosphatidylcholine monolayers. *Soft Matter 10*, 206−213.
(30) Gropp, C., Fischer, S., Husch, T., Trapp, N., Carreira, E. M., and Diederich, F. (2020) Molecular Recognition and Cocrystallization of Methylated and Halogenated Fragments of Danicalipin A by Enantiopure Alleno-Acetylenic Cage Receptors. *J. Am. Chem. Soc. 142*, 4749−4755.
(31) Krause, M. R., and Regen, S. L. (2014) The structural role of cholesterol in cell membranes: from condensed bilayers to lipid rafts. *Acc. Chem. Res. 47*, 3512−3521.

https://dx.doi.org/10.1021/acschembio.0c00624
ACS Chem. Biol. 2020, 15, 2986−2995

(32) Dufourc, E. J. (2008) Sterols and membrane dynamics. *J. Chem. Biol. 1*, 63−77.
(33) Hargreaves, W. R., Mulvihill, S. J., and Deamer, D. W. (1977) Synthesis of phospholipids and membranes in prebiotic conditions. *Nature 266*, 78−80.
(34) Hargreaves, W. R., and Deamer, D. W. (1978) Liposomes from ionic, single-chain amphiphiles. *Biochemistry 17*, 3759−3768.
(35) Mansy, S. S., Schrum, J. P., Krishnamurthy, M., Tobé, S., Treco, D. A., and Szostak, J. W. (2008) Template-directed synthesis of a genetic polymer in a model protocell. *Nature 454*, 122−125.
(36) Mansy, S. S. (2009) Model Protocells from Single-Chain Lipids. *Int. J. Mol. Sci. 10*, 835−843.
(37) Peters, G. H., et al. (2013) Binding of Serotonin to Lipid Membranes. *J. Am. Chem. Soc. 135* (6), 2164−2171.

https://dx.doi.org/10.1021/acschembio.0c00624
ACS Chem. Biol. 2020, 15, 2986−2995

Supporting Information

Halogenation-Dependent Effects of the Chlorosulfolipids of *Ochromonas Danica* on Lipid Bilayers

Frank R. Moss III,[†,‖] Gabrielle E. Cabrera,[†] Grace M. McKenna,[†] Giulio J. Salerno,[†,⊥] Steven R. Shuken,[†] Matthew L. Landry,[†,§] Thomas M. Weiss,[‡] Noah Z. Burns,[†,*] Steven G. Boxer[†,*]

† Department of Chemistry, Stanford University, Stanford, CA 94305, ‡ Stanford Synchrotron Radiation Laboratory, Stanford Linear Accelerator Center, Stanford University, Menlo Park, CA 94025

*To whom correspondence should be addressed:

1. General Information

All reactions were conducted in oven- or flame-dried glassware under an atmosphere of nitrogen or argon unless otherwise noted. Commercial reagents and solvents were used as received unless otherwise noted with the exception of the following: hexanes (ACS grade, 4.2% various methylpentanes), toluene, tetrahydrofuran, acetonitrile, methanol, benzene, and dichloromethane were dried by passing through a bed of activated alumina in a JC Meyer Solvent System. Flash column chromatography was performed using F60 silica gel (40-63 μm, 230- 400 mesh, 60Å) purchased from Silicycle. Analytical thin-layer chromatography (TLC) was carried out on 250 μm 60-F254 silica gel plates purchased from EMD Millipore, and visualization was effected by observation of fluorescence-quenching with ultraviolet light and staining with either *p*-anisaldehyde or phosphomolybdic acid (PMA) with cerium sulfate as a developing agent. Proton nuclear magnetic resonance (^{1}H NMR) and carbon nuclear magnetic resonance (^{13}C NMR) spectra were recorded on Varian Inova 600, Varian Inova 500, Varian Mercury 400, or Varian Inova 300 spectrometers operating respectively at 600, 500, 400, and 300 MHz for ^{1}H and at 150, 125, 100, and 75 MHz for ^{13}C. Chemical shifts are reported in parts per million (ppm) with respect to residual protonated solvent for ^{1}H (CDCl3 = δ 7.26, CD3OD = δ 3.31, DMSO-d6 = = δ 2.50) and with respect to carbon resonances of the solvent for ^{13}C (CDCl3 = δ 77.0, CD3OD = δ 49.0, DMSO-d6 = δ 39.5). Peak multiplicities are annotated as follows: app = apparent, br = broad, s = singlet, d = doublet, t = triplet, q = quartet, m = multiplet. Spectra were processed with exponential line broadening with a factor of 0.2. Infrared (IR) spectra were recorded on a Nicolet 6700 FT-IR spectrometer. LC-MS (ESI) data were collected on a Waters Micromass ZQ or a Waters Micromass LCT Premier mass spectrometer. GC-MS (CI) data were collected on a Waters Micromass GCT Premier mass spectrometer. Isotopic abundance patterns observed alongside each major ion reported matched calculated ratios. Optical rotations were measured using a JASCO P-2000 polarimeter. Chiral high-performance liquid chromatography (HPLC) analysis was performed using an Agilent 1260 with commercial ChiralPak 4.6 x 250 mm columns or a SpectraSystem P1000 with a SpectraSeries UV100 detector. HPLC trace integration was performed by the Agilent OpenLab processing suite. Uncorrected melting point data were collected using a Thomas Hoover Uni-Melt apparatus.

For biophysical experiments, phospholipids and algal lipids were from Avanti Polar Lipids. Texas Red 1,2-dihexadecanoyl-*sn*-glycero-3-phosphoethanolamine (Texas Red DHPE) was from Thermo Fisher Scientific. Solvents were from Thermo Fisher Scientific and were ACS grade and used as used as received. Four-inch ⟨100⟩ p-type silicon wafers were from Silicon Quest International. Other reagents were from Thermo Fisher Scientific unless otherwise noted. All water used was from a Millipore MilliQ system with a resistivity of ~18.2 MΩ·cm.

2. Synthesis of Sulfolipids

Scheme S1. Enantioselective Chemical Synthesis of Monochloro- and Deschloro-danicalipin A[a]

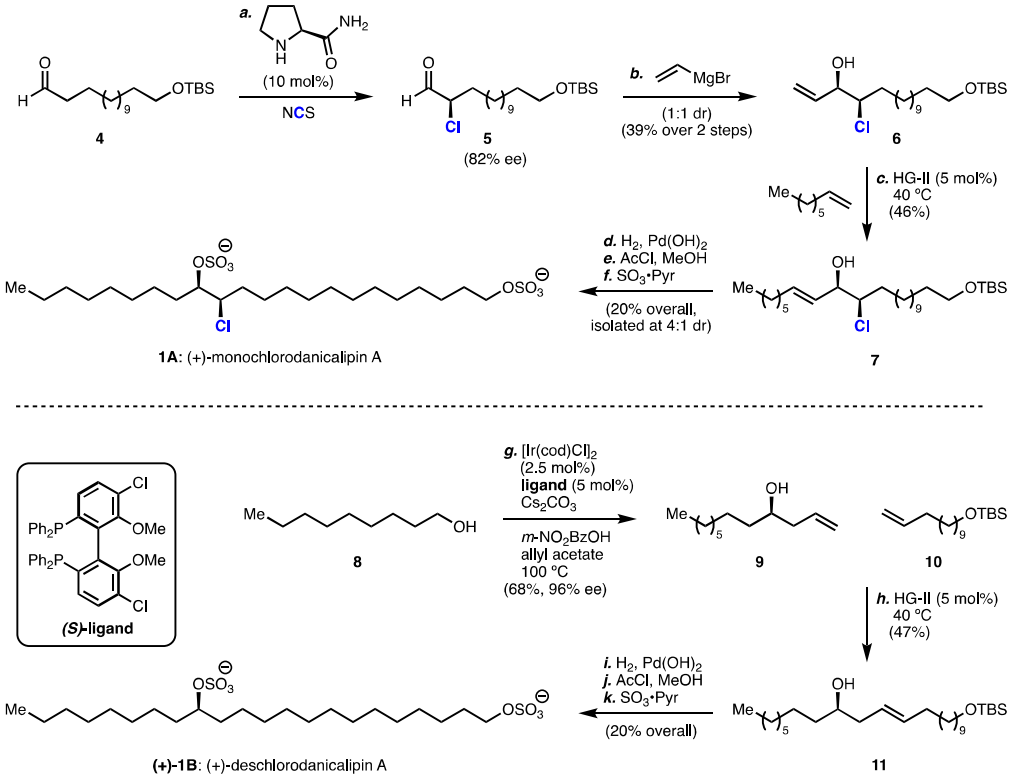

[a] Reagents and conditions: (a) **4** (1.0 equiv.), (*S*)-prolinamide (0.1 equiv.), NCS (1.3 equiv.), DCM, 0 ºC; (b) **5** (1.0 equiv.), vinylmagnesium bromide (1.0 equiv.), THF, –78 ºC, 39% yield over two steps, 82% *ee*; (c) **6** (1.0 equiv.), 1-octene (1.0 equiv.), Hoveyda-Grubbs II (0.05 equiv.), DCM, 40 ºC, 46%; (d) **7** (1.0 equiv), $Pd(OH)_2$ on carbon (0.1 equiv.), H_2 (1 atm), DCM/MeOH (1:1), rt; (e) AcCl (50 equiv.), MeOH, 0 ºC, 74% over two steps; (f) SO_3•Pyr (5.0 equiv.), DMF, rt, 31%; (g) **8** (1.0 equiv.), $[Ir(cod)Cl]_2$ (0.025 equiv.), (*S*)-ligand (0.05 equiv.), Cs_2CO_3 (0.2 equiv.), *m*-nitrobenzoic acid (0.1 equiv.), allyl acetate (10 equiv.), THF, 100 ºC, 68%, 92% *ee*; (h) **9** (1.0 equiv), **10** (1.0 equiv.), Hoveyda-Grubbs II (0.05 equiv.), DCM, 40 ºC, 47%; (i) **11** (1.0 equiv), $Pd(OH)_2$ on carbon (0.1 equiv.), H_2 (1 atm), DCM/MeOH (1:1), rt; (j) AcCl (50 equiv.), MeOH, 0 ºC, 82% over two steps; (k) SO_3•Pyr (10 equiv.), THF, rt, 24%. **(–)-1B** was prepared by the same route employing *(R)*-ligand.

Synthesis of monochlorodanicalipin A

The synthesis of monochlorodanicalipin A (**1A**) commenced from aldehyde **4** (available in 3 steps from commercially available materials). (*L*)-Prolinamide-catalyzed enantioselective chlorination of the aldehyde yielded the desired α-chloroaldehyde **5** in 82% *ee*.[1] Aldehyde **5** was carried directly into an organometallic addition with vinylmagnesium bromide, resulting in a 1:1 *dr* mixture of allylic alcohol **6**. Cross metathesis with 1-octene in the presence of catalytic Hoveyda-Grubbs II generated chlorohydrin **7** containing the full carbon framework of the natural product in 46% yield. Palladium-catalyzed hydrogenation and deprotection proceeded in 74% yield over two steps. Sulfation with sulfur trioxide pyridine complex

yielded monochlorodanicalipin A (**1A**) as a mixture of diastereomers in 34% yield. The diastereomeric mixture of lipids could be enriched to 4:1 dr via reverse phase preparative HPLC.

Synthesis of (+)- and (-)-deschlorodanicalipin A

The synthesis of deschlorodanicalipin A (**(+)-1B** and **(–)-1B**) commenced with the enantioselective allylation of nonanol **8** using a procedure developed by Krische.[2] The subsequent enantioenriched homoallylic alcohol **9** was isolated in 68% yield and 96% *ee* and was subjected to cross metathesis conditions with terminal alkene **10**, which was prepared in three steps from commercially available 1-bromodecanol allowing access to the fully elaborated chain **11** in 47% yield. Hydrogenation of **11** with catalytic palladium hydroxide and hydrogen gas proceeded quantitatively, followed by silyl deprotection under acidic conditions to yield the desired diol in 82% yield.[3] The product deschlorodanicalipin A (**(+)-1B** and **(–)-1B**) was isolated quantitatively following sulfation of the alcohols with sulfur trioxide pyridine complex, which proceeded in 24% yield.

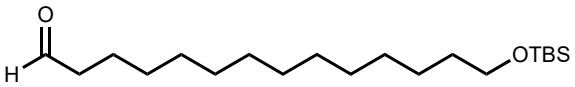

14-((tert-butyldimethylsilyl)oxy)tetradecanal (4)

Lithium aluminum hydride (1.54 g, 40.64 mmol, 2.1 equiv) was added portionwise to a mixture of 1,14-tetradecanedioic acid (5 g, 19.35 mmol, 1.0 equiv) in THF (200 mL) and stirred for 18 hours. The reaction was quenched with Rochelle salt (1.0 M solution, 100 mL) and stirred for 50 minutes. The reaction was extracted with EtOAc (100 mL), then the organic layer was washed with water (200 mL) and brine (200 mL) and dried with $MgSO_4$. The solution was concentrated *in vacuo*, and the diol crude product was used without further purification.

Sodium hydride (330 mg, 8.68 mmol, 1 equiv.) was added to diol (1.9 g, 8.68 mmol, 1.0 equiv.) in THF (64 mL) at room temperature. After 5 minutes, the reaction was heated briefly with a heat gun. TBS-Cl (1.24 g, 8.68 mmol, 1.0 equiv.) was added in one portion and the reaction was stirred for 12 hours. The reaction was quenched with NH_4Cl (saturated aq., 50 mL) and extracted with water and DCM. The solution was dried, concentrated, and purified by column chromatography (silica gel, 0 to 30% ethyl acetate in hexanes gradient) yielding the silyl protected product in 42% yield (1.62 g).

Sodium bicarbonate (177 mg, 2.1 mmol, 3.0 equiv.) and the alcohol substrate (242 mg, 0.70 mmol, 1.0 equiv.) were added to DCM (4 mL) under an atmosphere of air and cooled to 0°C. Dess-Martin's reagent (387 mg, 0.91 mmol, 1.3 equiv.) was added portion-wise and the reaction is allowed to stir for 10 minutes, then warmed to room temperature and stirred for another 30 minutes. While stirring, the solution is then diluted with hexanes and washed with saturated $NaHCO_3$ (5 mL). The organic layer is dried with $MgSO_4$, concentrated, and purified by column chromatography (silica gel, 0 to 15% ethyl acetate in hexanes gradient) to provide **4** in 40% yield over 3 steps (240 mg). The product was spectroscopically in agreement with that previously reported.[4]

Physical properties: Clear, colorless oil;

R_f = 0.30 (silica gel, 10% ethyl acetate in hexanes, visualized with anisaldehyde stain);

^{1}H NMR (400 MHz, $CDCl_3$) δ 9.76 (t, *J* = 1.9 Hz, 1H), 3.59 (t, *J* = 6.7 Hz, 2H), 2.42 (td, *J* = 7.4, 2.0 Hz, 2H), 1.57 – 1.45 (m, 2H), 1.27 (m, 18H), 0.89 (s, 9H), 0.05 (s, 6H).

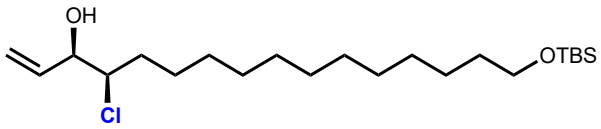

(13*R*,14*R*)-1-((tert-butyldimethylsilyl)oxy)-13-chloro-15-hexadecen-14-ol (6)

Based on a preparation developed by Jørgenson and coworkers,[5] a solution of **4** (297 mg, 0.87 mmol, 1.0 equiv.) in DCM (3.4 mL) was cooled to 0°C. *(S)*-Prolinamide (9.9 mg, 0.09 mmol, 0.1 equiv.) and NCS (150 mg, 1.13 mmol, 1.3 equiv.) were added and the solution was stirred for 1 hour at 0°C. the reaction was warmed slowly to room temperature over 3 hours and stirred to completion. The solution was diluted with hexanes and filtered. The filtrate was concentrated, dissolved in hexanes, filtered, and concentrated again. An aliquot of the reaction was treated with NaBH4, and the resulting alcohol was trapped as the benzoate ester for analysis of enantiomeric enrichment via chiral HPLC. The crude α-chloroaldehyde (**5**) was used without further purification.

A solution of crude α-chloroaldehyde (**5**) in THF (6 mL) was cooled to -78°C. Vinylmagnesium bromide (1M in Et_2O, 0.87 mL, 0.87 mmol, 1.0 equiv.) was slowly added and the solution was warmed to room temperature and stirred for 20 hours. The solution was quenched with NH_4Cl (25 mL), diluted with Et_2O (25 mL), and the layers separated. The aqueous layer was extracted with Et_2O (2 x 25 mL) and the combined organics were washed with brine (50 mL). The organic layer was dried over $MgSO_4$, filtered, and concentrated *in vacuo*. The crude was purified by flash column chromatography (silica gel, 40 to 100% DCM in hexanes gradient) to provide **6** in 39% yield over two steps at a 1:1 mixture of diastereomers (137 mg, 82% ee).

Physical properties: Clear, colorless oil;

R_f = 0.40 (silica gel, 60% dichloromethane in hexanes, visualized with anisaldehyde stain);

IR (film) ν_{max} 2924, 2854, 2177, 2023, 1463, 1254, 1099, 835, 775 cm^{-1};

^{1}H NMR (600 MHz, $CDCl_3$) δ 5.97 – 5.84 (m, 1H), 5.41 – 5.21 (m, 2H), 4.17 (t, *J* = 5.5 Hz, 1H), 3.90 (dt, *J* = 9.3, 4.5 Hz, 1H), 3.59 (t, *J* = 6.7 Hz, 2H), 1.88 – 1.80 (m, 1H), 1.74 (dtt, *J* = 15.5, 10.2, 5.1 Hz, 2H), 1.50 (q, *J* = 6.8 Hz, 2H), 1.27 (m, *J* = 9.8 Hz, 18H), 0.89 (s, 9H), 0.05 (s, 6H);

^{13}C NMR (126 MHz, $CDCl_3$) δ 136.97, 117.57, 75.31, 68.28, 63.25, 34.26, 32.79,29.60, 29.52, 29.48, 29.42, 29.34, 29.34, 28.96, 26.40, 25.89, 25.70, 18.28, -5.35;

LC-MS (ESI) calcd. for $C_{22}H_{45}{}^{35}ClNaO_2Si^+$: 427.28, found 427.30;

$[\alpha]_D^{23}$ = 18.08 (c = 0.31, $CHCl_3$) (at 82% ee).

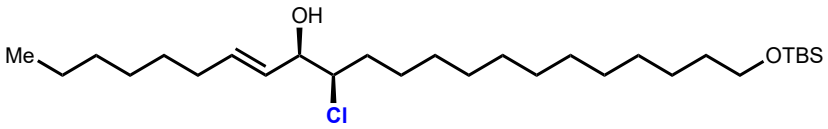

(13*R*,14*R*)-1-((tert-butyldimethylsilyl)oxy)13-chloro-15-docosen-14-ol (7)

Hoveyda-Grubbs II catalyst (2.4 mg, 0.0038 mmol, 0.05 equiv.) was added to a solution of **6** (31 mg, 0.076 mmol, 1.0 equiv.) and 1-octene (0.012 mL, 0.076 mmol, 1.0 equiv.) in degassed DCM. The solution was stirred at 40°C for 24 hours. The solvent was concentrated *in vacuo* and the crude residue purified by flash column chromatography (silica gel, 20 to 70% DCM in hexanes gradient) to provide **7** in 46% yield (17 mg).

Physical properties: Clear, colorless oil;

R_f = 0.60 (silica gel, 50% dichloromethane in hexanes, visualized with anisaldehyde stain);

IR (film) ν_{max} 3403, 2923, 2853, 1462, 1386, 1252, 1097, 1005, 968, 938, 833, 773, 721, 661 cm^{-1};

^{1}H NMR (600 MHz, $CDCl_3$) δ 5.78 (dt, *J* = 14.4, 6.8 Hz, 1H), 5.52 – 5.42 (m, 1H), 4.08 (t, *J* = 6.4 Hz, 1H), 3.86 (ddd, *J* = 9.5, 5.6, 3.9 Hz, 1H), 3.59 (t, *J* = 6.6 Hz, 2H), 2.06 (q, *J* = 7.3 Hz, 2H), 1.69 (dtd, *J* = 14.3, 9.7, 4.6 Hz, 3H), 1.50 (m, *J* = 6.8 Hz, 3H), 1.35 – 1.25 (m, 28H), 0.89 (s, 9H), 0.05 (s, 6H);

^{13}C NMR (126 MHz, $CDCl_3$) δ 135.53, 128.66, 75.84, 69.25, 63.50, 34.53, 33.44, 33.04, 32.44, 31.82, 29.78, 29.74, 29.69, 29.59, 29.25, 29.07, 28.96, 26.76, 26.57, 26.14, 25.95, 22.76, 18.53, 14.22, -5.11**;**

LC-MS (ESI) calcd. for $C_{28}H_{58}{}^{35}ClNaO_2Si^+$: 511.37, found 511.4;

$[\alpha]_D^{23}$ = 11.53 (c = 0.34, $CHCl_3$) (at 82% ee).

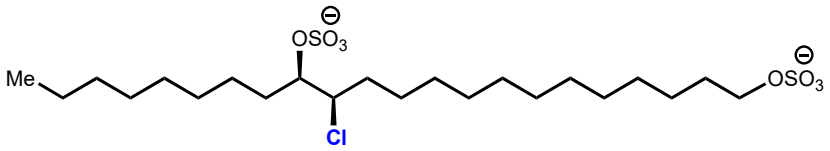

(13*R*,14*R*)-13-chlorodocosane-1,14-diyl bis(sulfate) (1A)

7 (17 mg, 0.035 mmol, 1.0 equiv) and palladium(II) hydroxide on carbon (0.5 mg, 0.0035 mmol, 0.1 equiv) were added to a 1:1 mixture of anhydrous CH_2Cl_2 (0.35 mL) and MeOH (0.35 mL). The resulting solution was degassed with N_2 for 10 minutes, followed by H_2 for another 10 minutes. The reaction was stirred for 30 minutes under an atmosphere or H_2. The mixture was filtered through Celite and the residue is washed with CH_2Cl_2 and MeOH and the filtrate was concentrated.

The crude product is dissolved in MeOH (1.27 mL) and cooled to 0°C. Acetyl chloride (0.13 mL, 1.75 mmol, 50 equiv) was added dropwise and the solution was stirred at room temperature for 12 hours and quenched with $NaHCO_3$ (10%, 1ml) and washed with water (2 mL). The organic layer was dried with $MgSO_4$ and concentrated, and the crude residue was purified via column chromatography (silica gel, 10 to 50% EtOAc in hexanes gradient) to provide the desired diol in 74% yield over two steps (10 mg).

Sulfur trioxide-pyridine complex (42 mg, 0.13 mmol, 5.0 equiv) was added to a stirring solution of the chloro-diol (10 mg, 0.027 mmol, 1.0 equiv) in DMF (2 mL). After 14 hours the solution was concentrated and filtered through a plug of silica, washing with 20% MeOH in CH_2Cl_2. The crude residue was purified via column chromatography (silica gel, 0 to 20% MeOH in DCM gradient) to provide **1A** in 31% yield as a 1:1 mix of diastereomers (4.5 mg). This mixture could be enriched to a 4:1 mix of diastereomers via reverse phase preparative HPLC (C18 column, 0-100% H_2O:CH_3CN, 60 minutes, 5 mL/min). The product was spectroscopically in agreement with that previously reported.[6]

Physical properties: Clear, colorless oil;

R_f = 0.15 (silica gel, 10% MeOH in DCM, visualized with Seebach's stain);

^{1}H NMR (600 MHz, CD_3OD) δ 4.42 (dt, *J* = 8.2, 3.8 Hz, 1H), 4.29 (dt, *J* = 10.4, 3.1 Hz, 1H), 3.99 (t, *J* = 6.7 Hz, 2H), 1.98 – 1.92 (m, 1H), 1.86 – 1.78 (m, 1H), 1.70 – 1.57 (m, 6H), 1.44 – 1.25 (m, 28H), 0.90 (t, *J* = 7.0 Hz, 3H).

$[\alpha]_D^{23}$ = 13.26 (c = 0.14, MeOH) (at 82% ee).

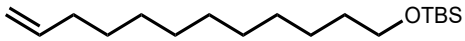

1-((*tert*-butyldimethylsilyl)oxy)-11-dodecene (10)

Hydrobromic acid (12 mL, 68.8 mmol, 1.2 equiv.) was added to a solution of 1,10-decanediol (10 g, 57.4 mmol, 1.0 equiv.) in toluene (150 mL) and heated at reflux for 14 hours. The solution was cooled to room temperature, then diluted with Et_2O (50 mL), and quenched with 1M NaOH (10 mL). The layers were separated, and the organic layer was washed with brine (100 mL) and dried with $MgSO_4$. The mixture was filtered, concentrated *in vacuo* and purified by flash chromatography (silica gel, 20 to 70% Et_2O in hexanes gradient) providing 1-bromo-10-decanol in 74% yield (10.1 g).

TBSCl was added to a solution of bromoalcohol (7.67 g, 50.9 mmol, 1.2 equiv.) in DCM (216 mL). Imidazole (4.33 g, 63.6 mmol, 1.5 equiv.) and DMAP (518 mg, 4.2 mmol, 0.1 equiv.) were added and the solution was stirred for 12 hours. The reaction was quenched with absolute ethanol (3 mL), then washed with saturated NH_4Cl (200 mL). The aqueous layer was washed with EtOAc (2 x 150 mL), then the organic layers were combined, washed with brine (300 mL), and dried with Na_2SO_4. The organic layer was concentrated and redissolved in acetone (86.5 mL). NaI (32.38 g, 216 mmol, 5.0 equiv) was added and the solution was stirred for 12 hours. The solution was then diluted with hexanes (30 mL) and washed with water (2 x 100 mL). The aqueous layer was extracted with hexanes (2 x 100 mL) and the combined organic layers were concentrated. The residue was diluted with hexanes (50 mL), filtered with a short pad of Celite, and concentrated under reduced pressure to yield the silyl protected product in 78% yield (13.1 g).

Copper (I) iodide (476 mg, 2.5 mmol, 1.0 equiv.) and THF (5 mL) were added to a flame dried flask. A solution of vinylmagnesium bromide (1 M, 5.36 mL, 7.5 mmol, 3 equiv.) was added and the solution was stirred at -40° for 15 minutes. A solution of alkyl bromide (1 g, 2.5 mmol, 1.0 equiv.) in THF (5 mL), HMPA (0.87 mL, 5.0 mmol, 2.0 equiv.), and triethyl phosphite (0.86 mL, 5 mmol, 2 equiv.) were added and the mixture was stirred for 1 hour. The reaction was warmed to room temperature and stirred for an additional 2 hours, then quenched with NH_4Cl (10 mL). The aqueous layer was separated and extracted with EtOAc (10 mL), washed with brine (7 mL), and dried over $MgSO_4$. The mixture was filtered, concentrated under reduced pressure, and purified by flash column chromatography (silica gel, 0 to 20% Et_2O in hexanes gradient) providing **10** in 77% yield (577 mg). The product was spectroscopically in agreement with that previously reported.[7]

Physical properties: Clear, colorless oil;

R_f = 0.60 (silica gel, 10% diethyl ether in hexanes, visualized with Seebach's stain);

^{1}H NMR (400 MHz, $CDCl_3$) δ 5.81 (ddt, *J* = 16.9, 10.2, 6.7 Hz, 1H), 5.04 – 4.89 (m, 2H), 3.60 (t, *J* = 6.6 Hz, 2H), 2.04 (tdd, *J* = 8.1, 6.0, 1.4 Hz, 2H), 1.54 – 1.48 (m, 2H), 1.36 – 1.25 (m, 14H), 0.89 (s, 9H), 0.04 (s, 6H).

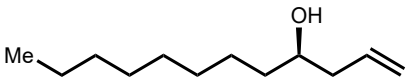

(4*R*)-1-Dodecen-4-ol ((+)-9)

Following a procedure disclosed by Krische and coworkers,[2] 1-nonanol (1.29 mL, 7.4 mmol, 1 equiv.) and THF (18 mL) were added to an oven-dried sealed tube. $[Ir(cod)Cl]_2$ (124 mg, 0.19 mmol, 0.025 equiv.), (*S*)-Cl,MeO-BIPHEP (241 mg, 0.37 mmol, 0.05 equiv.), Cs_2CO_3 (481 mg, 1.48 mmol, 0.2 equiv.), and *m*-nitrobenzoic acid (123 mg, 0.74 mmol, 0.1 equiv.) are added followed by allyl acetate (7.97 mL, 73.8 mmol, 10 equiv.). The reaction mixture was allowed to stir at 100°C for 20 hours. The reaction was cooled to room temperature, concentrated onto silica gel, and purified by flash column chromatography (silica gel, 5 to 40% Et_2O in hexanes gradient) to provide **9** in 68% yield (916 mg, 96% ee). The product was spectroscopically in agreement with that previously reported.[2] Enantioenrichment was quantified by chiral HPLC of the 4-nitrobenzoate ester (see below).

Physical properties: Clear, colorless oil;

R_f = 0.20 (silica gel, 10% diethyl ether in hexanes, visualized with Seebach's stain);

^{1}H NMR (600 MHz, $CDCl_3$) δ 5.88 – 5.78 (m, 1H), 5.17 – 5.10 (m, 2H), 3.64 (m, 1H), 2.34 – 2.26 (m, 1H), 2.14 (dtt, *J* = 14.0, 7.9, 1.1 Hz, 1H), 1.54 (br s, 1H), 1.50 – 1.41 (m, 3H), 1.36 – 1.23 (m, 11H), 0.88 (t, *J* = 7.0 Hz, 3H);

$[\alpha]_D^{23}$ =7.75 (c = 0.46, $CHCl_3$) (at 96% ee).

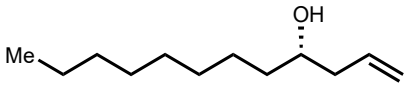

(4*S*)-1-Dodecen-4-ol ((–)-9)

$[\alpha]_D^{23}$ = -8.93 (c = 0.32, $CHCl_3$) (at 96% ee).

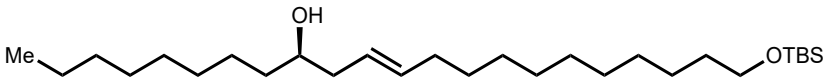

***E*-(14R)-1-((*tert*-butyldimethylsilyl)oxy)-11-docosen-14-ol ((+)-11)**

Hoveyda-Grubbs II catalyst (18 mg, 0.029 mmol, 0.05 equiv.) was added to a solution of **9** (301 mg, 1.64 mmol, 1.0 equiv.) and **10** (488 mg, 1.64 mmol, 1.0 equiv.) in degassed DCM. The solution was stirred at 40°C for 24 hours. The solvent was concentrated *in vacuo* and purified by flash column chromatography (silica gel, 0 to 20% EtOAc in hexanes gradient) to provide **11** in 47% yield (350 mg).

Physical properties: Clear, colorless oil;

R_f = 0.50 (silica gel, 10% ethyl acetate in hexanes, visualized with Seebach's stain);

IR (film) ν_{max} 3363, 2919, 2850, 1463, 1388, 1359, 1253, 1097, 1005, 959, 833, 723, 720, 663 cm^{-1};

^{1}H NMR (600 MHz, $CDCl_3$) δ 5.53 (dt, *J* = 15.2, 6.6 Hz, 1H), 5.43 – 5.35 (m, 1H), 3.59 (t, *J* = 6.7 Hz, 2H), 3.57 (s, 1H), 2.26 – 2.18 (m, 1H), 2.03 (dq, *J* = 27.1, 7.5 Hz, 3H), 1.63 (br s, 1H), 1.52 – 1.43 (m, 2H), 1.46 – 1.39 (m, 3H), 1.37 – 1.32 (m, 2H), 1.27 (d, *J* = 10.2 Hz, 24H), 0.88 (d, *J* = 9.0 Hz, 11H), 0.04 (s, 6H).

^{13}C NMR (101 MHz, $CDCl_3$) δ 134.89, 125.95, 71.04, 63.45, 40.87, 36.87, 33.03, 32.82, 32.03, 29.85, 29.78, 29.73, 29.71, 29.67, 29.62, 29.58, 29.47, 29.43, 29.33, 26.13, 25.95, 25.84, 22.82, 18.52, 14.25, -5.12.

LC-MS (ESI) calcd. for $C_8H_{14}{}^{35}Cl_2O[NH_4]^+$:455.43, found 455.48;

$[\alpha]_D^{23}$ = 1.02 (c = 0.47, $CHCl_3$) (at 96% ee).

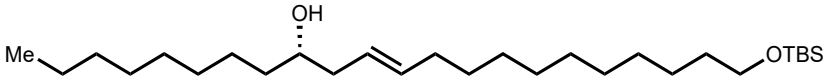

***E*-(14S)-1-((*tert*-butyldimethylsilyl)oxy)-11-docosen-14-ol ((–)-11)**

$[\alpha]_D^{23}$ = -1.30 (c = 0.41, $CHCl_3$) (at 96% ee).

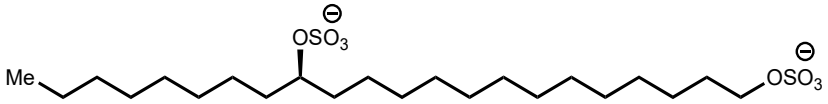

(*R*)-docosane-1,14-diyl bis(sulfate) ((+)-1B)

Based on analogous work by Carreira and coworkers,[8] **11** (292 mg, 0.642 mmol, 1.0 equiv.) and palladium(II) hydroxide on carbon (9.01 mg, .064 mmol, 0.1 equiv.) were added to a 1:1 mixture of anhydrous CH_2Cl_2 (7 mL) and MeOH (7 mL). The resulting solution was degassed with N_2 for 10 minutes, followed by H_2 for another 10 minutes. The reaction was stirred for 30 minutes under an atmosphere or H_2. The mixture was filtered through Celite and the residue is washed with CH_2Cl_2 and MeOH and the filtrate was concentrated.

The crude product is dissolved in MeOH (26 mL) and cooled to 0°C. Acetyl chloride (0.91 ml, 12.8 mmol, 20 equiv.) was added dropwise and the solution was stirred at room temperature for 12 hours and quenched with $NaHCO_3$ (10 wt%, 8 mL) and washed with water (15 mL). The organic layer was dried with $MgSO_4$ and concentrated, and the crude residue was purified via column chromatography (silica gel, 10 to 50% EtOAc in hexanes gradient) to provide the diol product in 82% yield (180 mg).

Sulfur trioxide-pyridine complex (404 mg, 2.54 mmol, 10.0 equiv.) was added to a stirring solution of the diol (174 mg, 0.51 mmol, 1.0 equiv.) in THF. After 14 hours the solution was concentrated and filtered through a plug of silica, washing with 20% MeOH in CH_2Cl_2. The crude residue was purified via column chromatography (silica gel, 0 to 20% MeOH in DCM gradient) to provide **1B** in 24% yield (61 mg). The product was spectroscopically in agreement with that previously reported.[3]

Physical properties: Clear, colorless oil;

R_f = 0.11 (silica gel, 10% MeOH in DCM, visualized with Seebach's stain);

^{1}H NMR (600 MHz, CD_3OD) δ 4.34 (p, *J* = 6.0 Hz, 1H), 4.00 (t, *J* = 6.5 Hz, 2H), 1.70 – 1.57 (m, 7H), 1.41-1.24 (m, 31H), 0.90 (d, *J* = 13.9 Hz, 3H).

$[\alpha]_D^{23}$ = 2.25 (c = 0.39, $CHCl_3$) (at 96% ee).

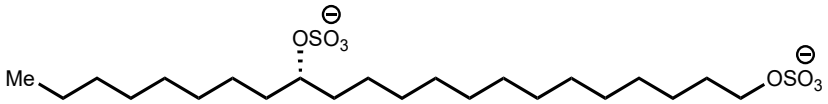

(*S*)-docosane-1,14-diyl bis(sulfate) ((–)-1B)

$[\alpha]_D^{23}$ = -0.36 (c = 0.34, MeOH) (at 96% ee).

3. Synthesis of (+)-danicalipin A

Scheme S2. Enantioselective Chemical Synthesis of Danicalipin A

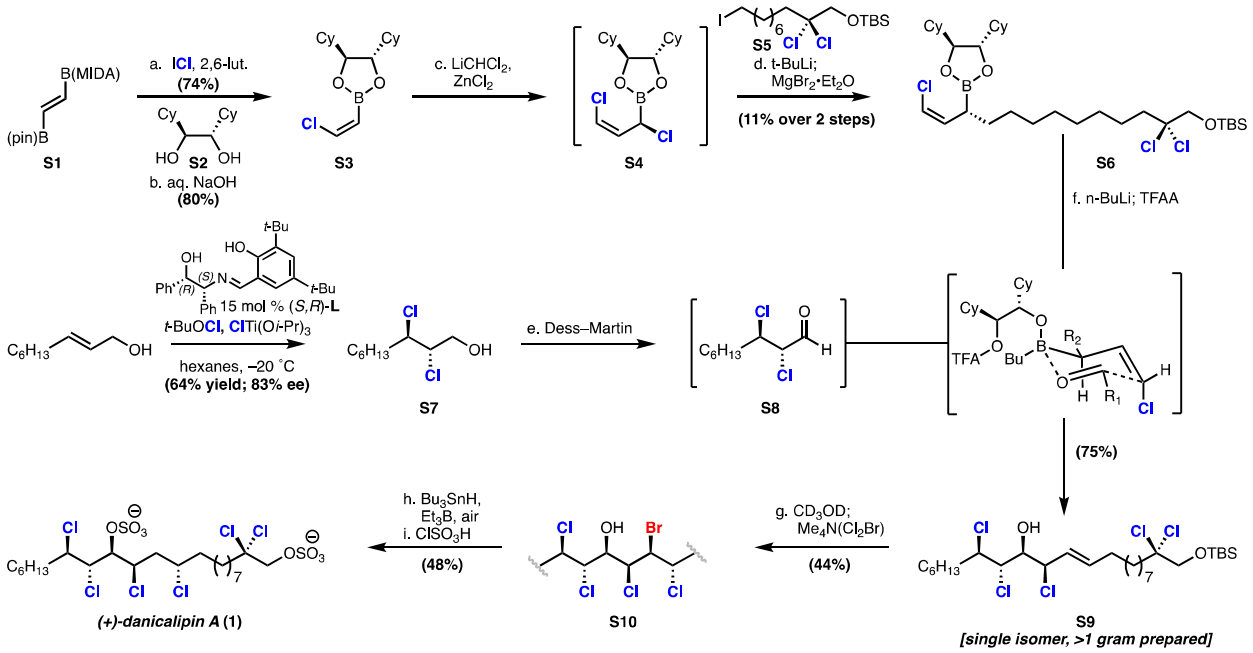

We synthesized (+)-dancalipin A by modifying a previously published route to (–)-danicalipin A.[9] The natural enantiomer (+)-danicalipin A (**1**) was synthesized via the same route employing ***ent*-S2** and (*S,R*)-**L**. The synthesis of (+)-danicalipin A was performed by first accessing the desired (*Z*)-chlorovinylboron reagent via a sequence inspired by the preparation of a related (*Z*)-(2-bromovinyl)-MIDA developed by Burke.[Error! Bookmark not defined.,10] Treatment of commercially available **S1** with iodine monochloride and 2,6-lutidine yielded (*Z*)-(2-chlorovinyl)-MIDA, which could undergo facile ligand exchange with commercially available enantiopure chiral diol **S2** to yield the desired (*Z*)-chlorovinylboronic ester. Preparation of the fully elaborated chiral allylboron reagent was achieved via a two-step homologation sequence. Using conditions originally developed by Matteson, **S3** was treated with dichloromethyllithum followed by zinc chloride to yield a 1,3-dichloroallylboronic ester which was chromatographically unstable.[11,12,13] Subsequent treatment of this crude compound with the *in situ* generated Grignard reagent of alkyl iodide **S5** to yield the fully functionalized chiral allylbornic ester **S6**, which was deteremined to be >99% ee via Mosher ester analysis of the corresponding alcohol. With access to the chloroallyl boronic ester **S6**, allylation of the enriched dichloroaldehyde **S8** was attempted. It was found that using an activation procedure of the boronic ester developed by Aggarwal to the borinate via the addition of *n*-butyllithium and trifluoroacetic acid the fully elaborated chlorohydrin **S9** was accessible in 75% yield.[14,15] Further analysis showed that a kinetic resolution occurs during this chloroallylation reaction, and thus **S9** was isolated as a *single enantio- and diastereomer*. A formal hydrochlorination of the alkene was affected by a two-step sequence, with initial bromochlorination of the *O*-deuterated **S9** with $Me_4N(Cl_2Br)$ in 44% yield.[16,17] Subsequent radical

debromination with tributyltin hydride proceeded in 74% yield based on recovered starting material. Sulfation yielded (+)-danicalipin A (**1**) in 8 linear steps.

4. ^{1}H and ^{13}C NMR Spectra

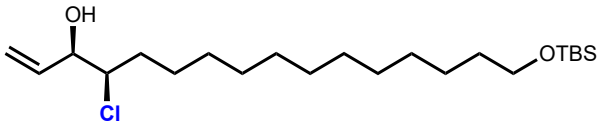

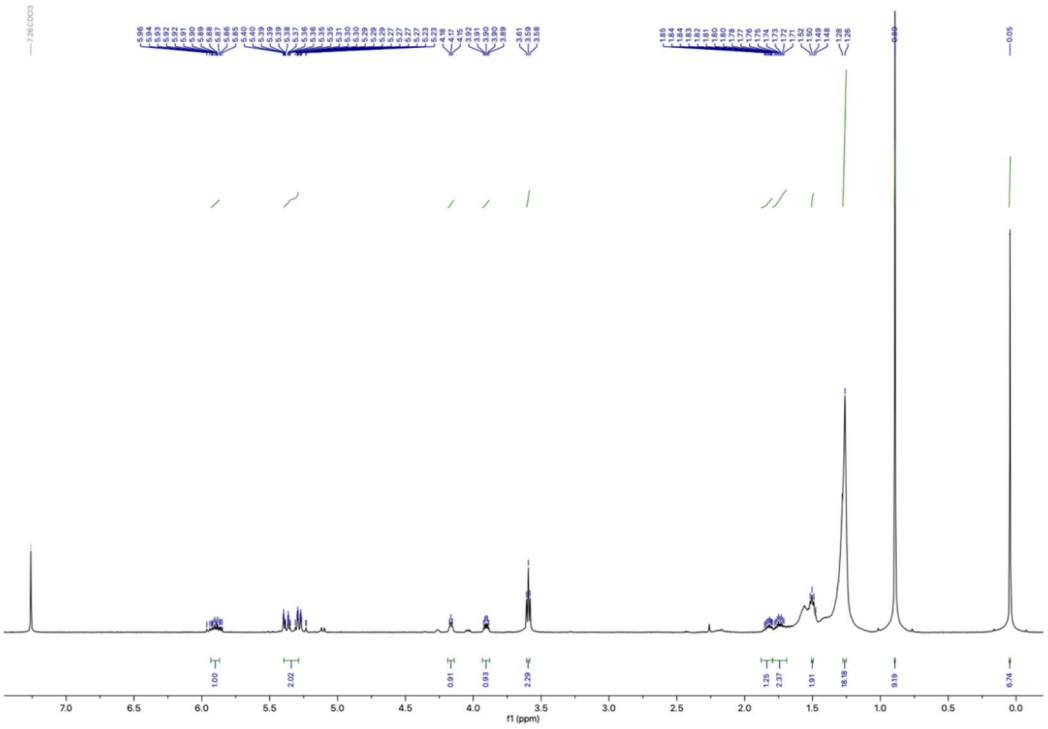

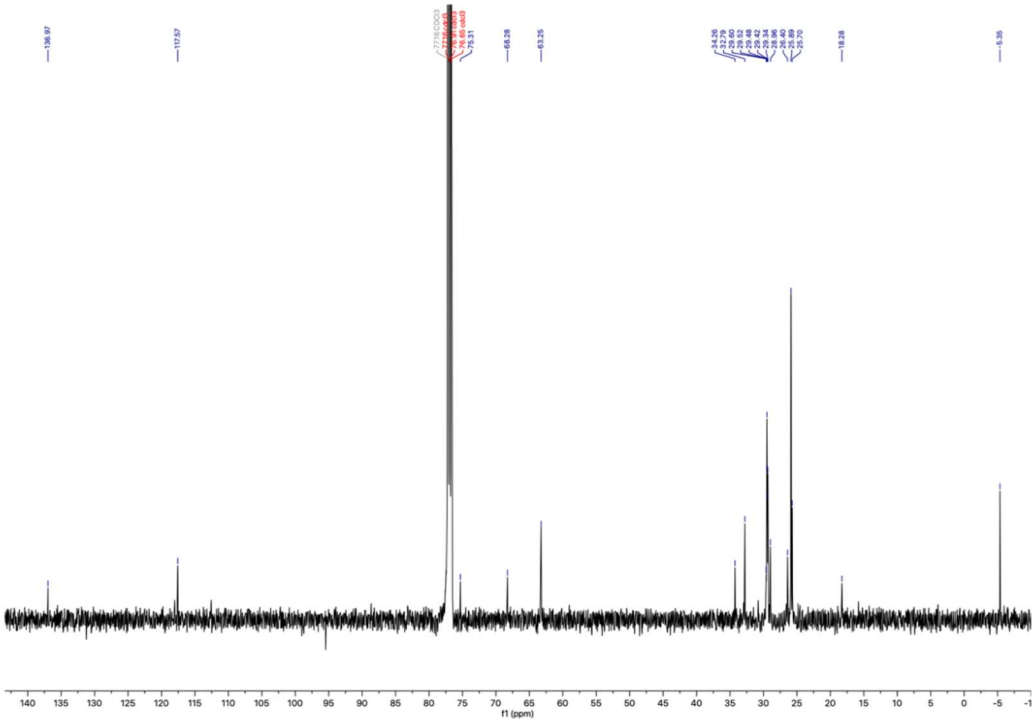

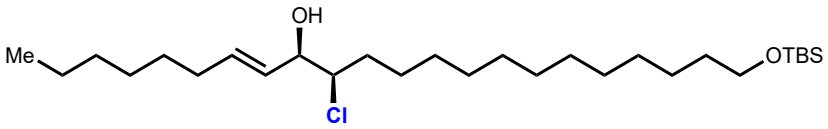
OH
Me
OTBS
Cl

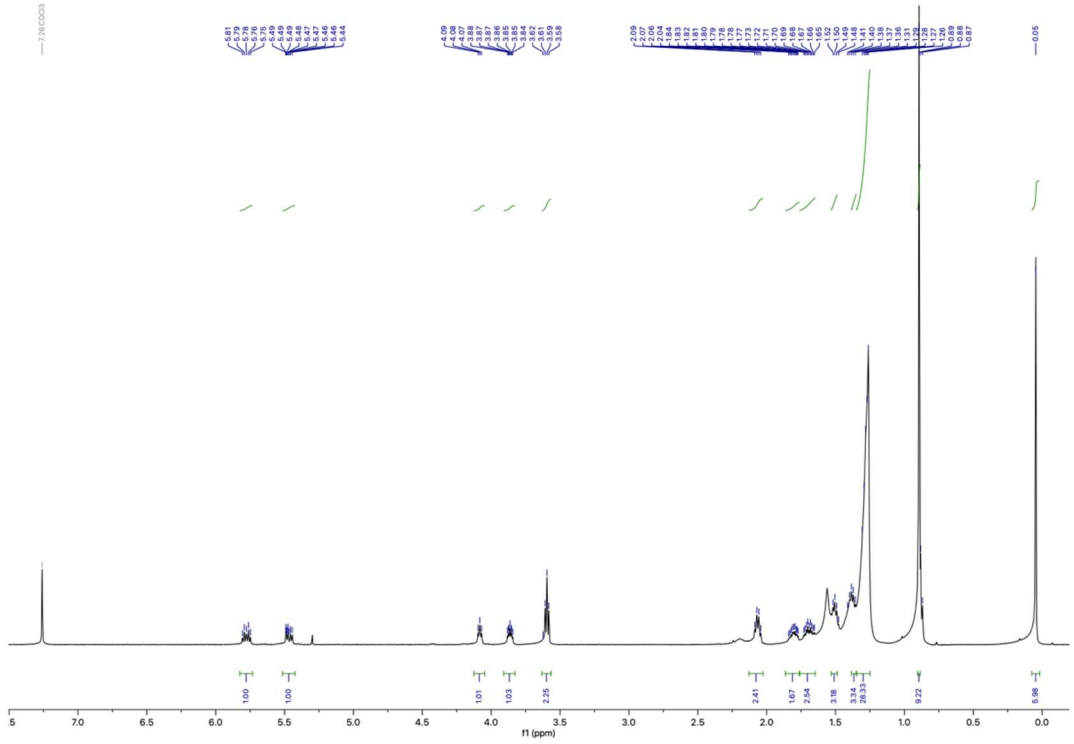
f1 (ppm)

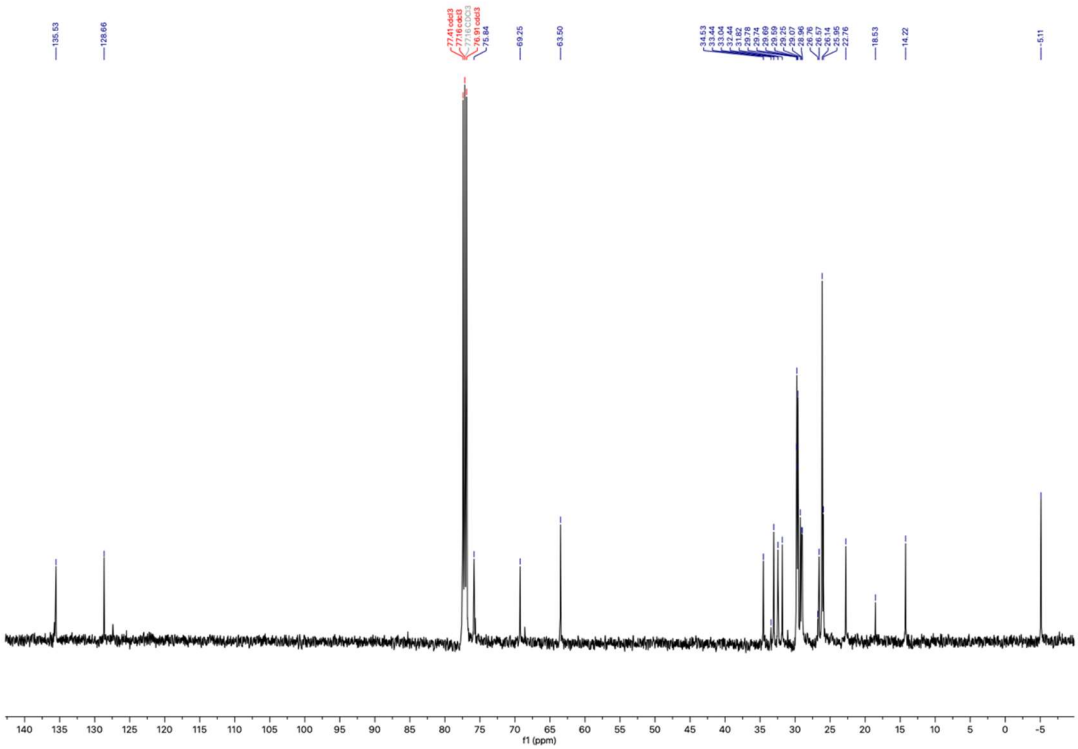
f1 (ppm)

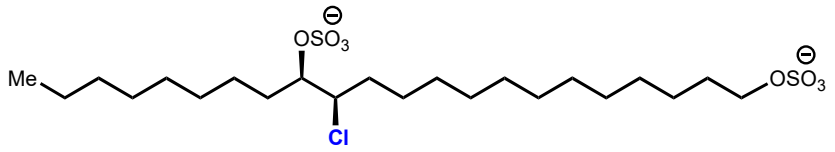
Me
OSO3
OSO3
Cl

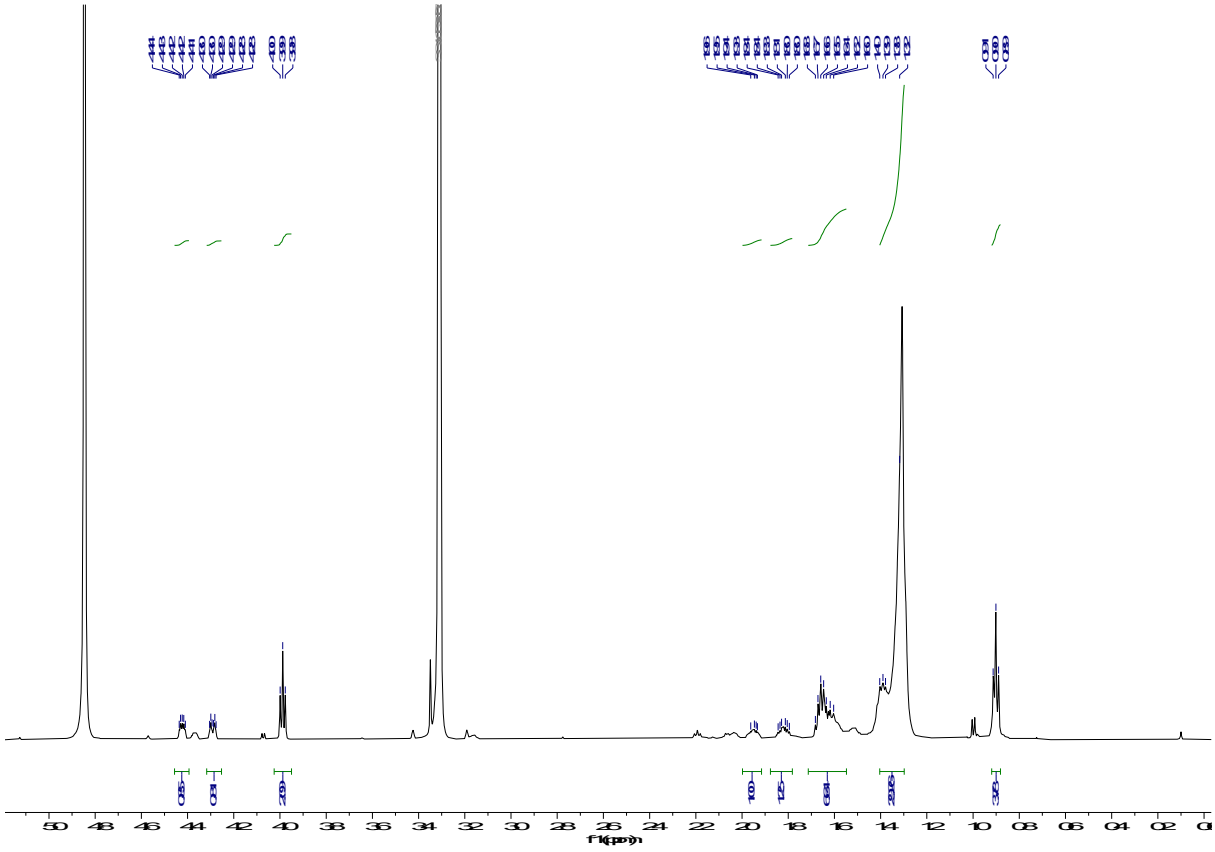

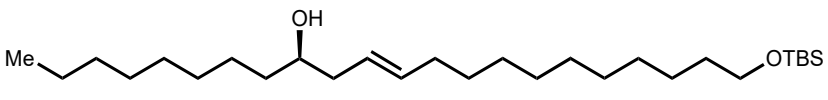
OH
Me
OTBS

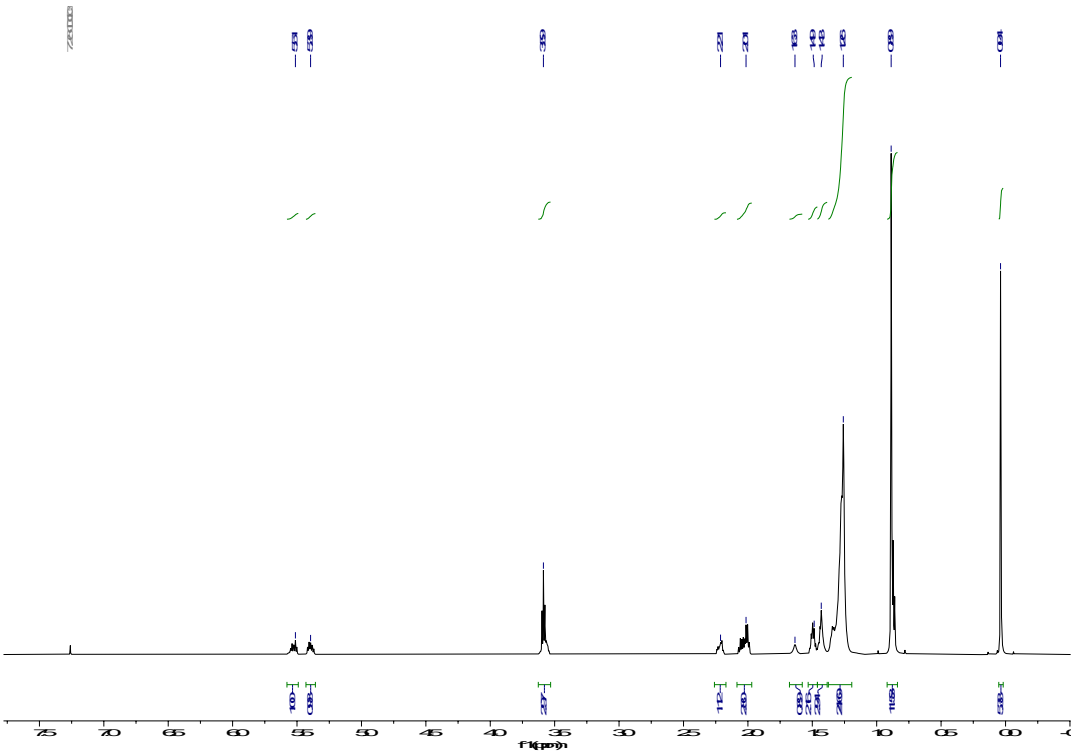

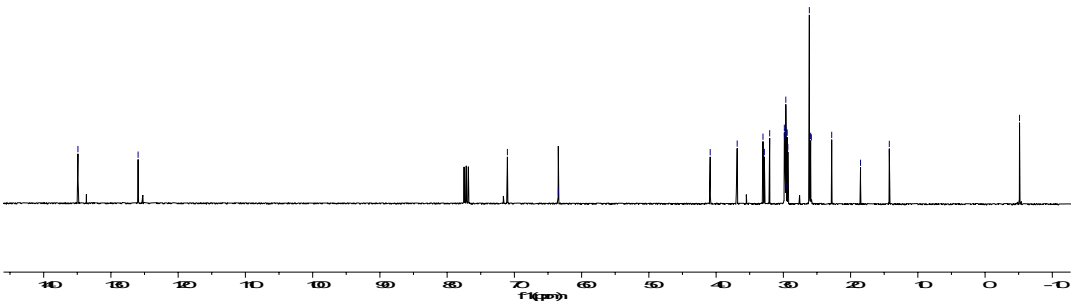

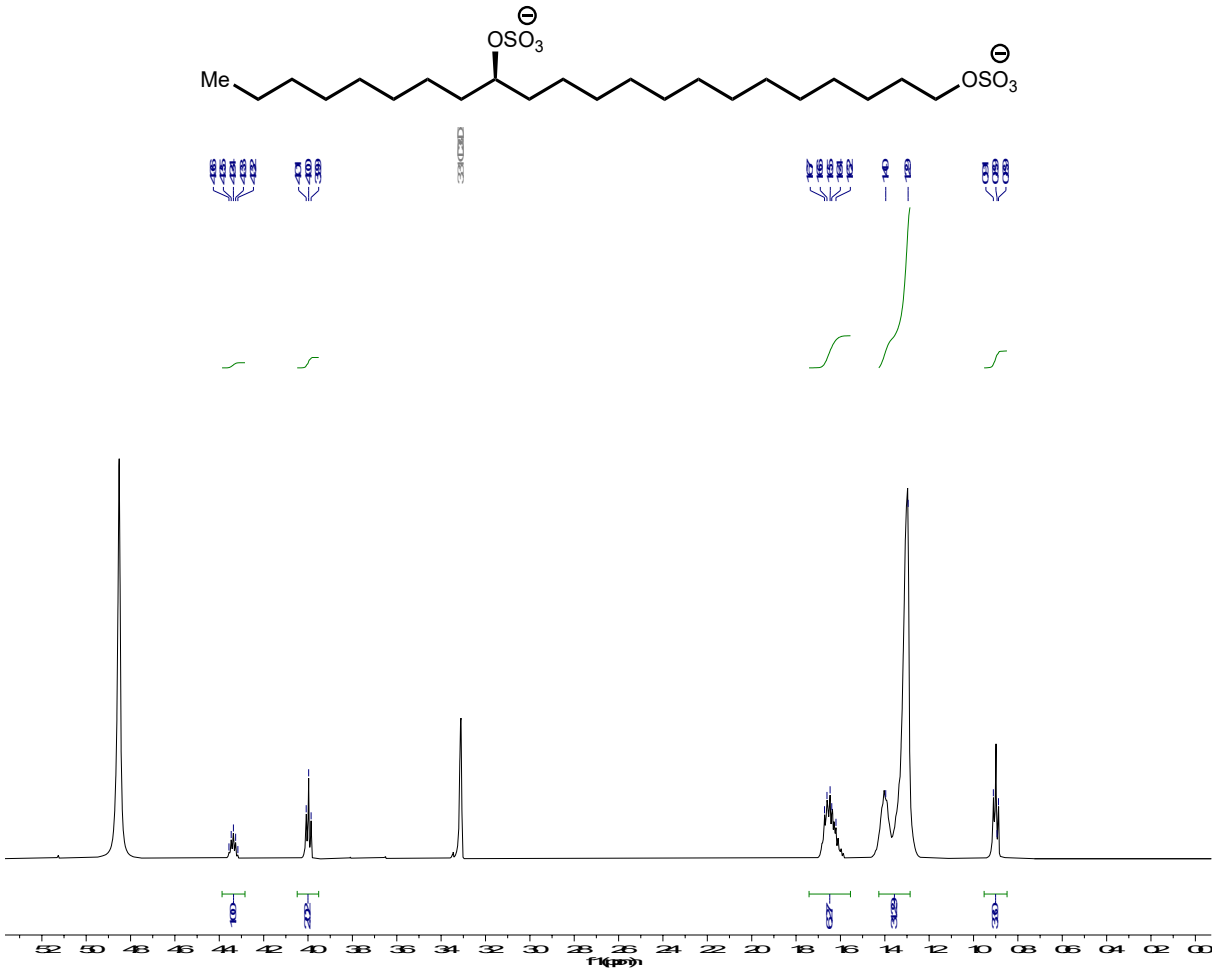
OSO3
Me
OSO3

5. HPLC Traces

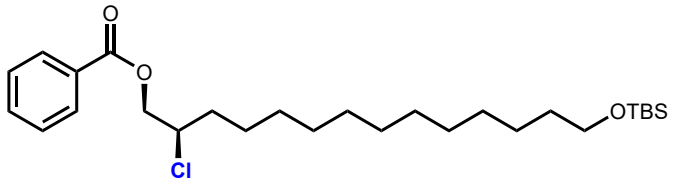

Racemic Sample: Chiralpak OD-H column, 0.25% *i*-PrOH in Hexanes, 30 minutes

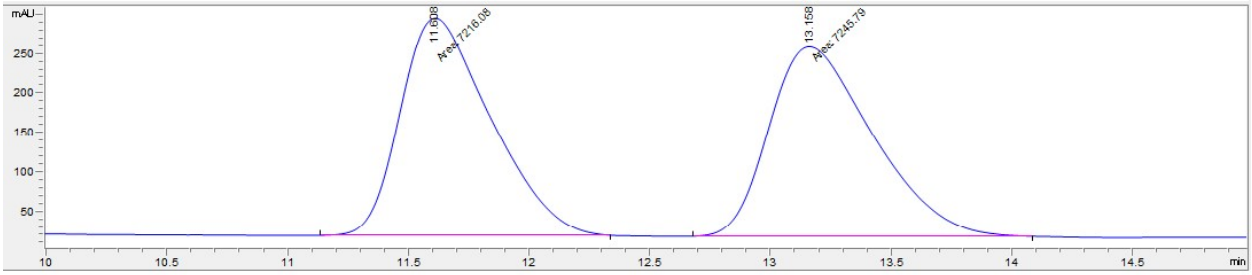

Peak #	RetTime [min]	Type	Width [min]	Area [mAU*s]	Height [mAU]	Area %
1	11.608	MM	0.4352	7216.07910	276.33786	49.8973
2	13.158	MM	0.5007	7245.79053	241.20280	50.1027

Scalemic Sample: Chiralpak OD-H column, 0.25% *i*-PrOH in Hexanes, 30 minutes

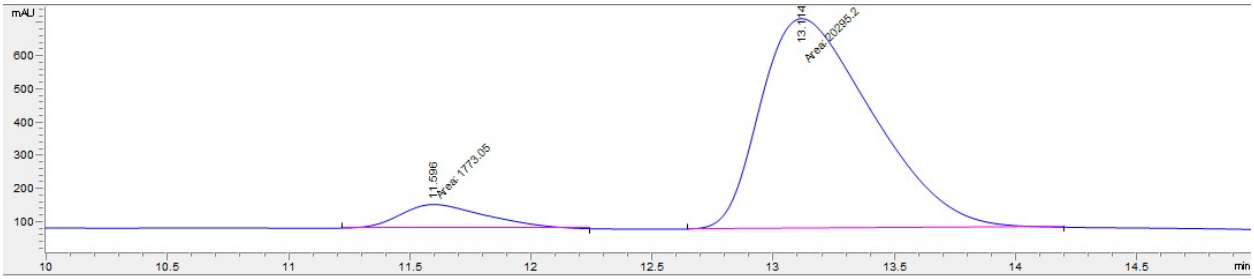

Peak #	RetTime [min]	Type	Width [min]	Area [mAU*s]	Height [mAU]	Area %
1	11.596	MM	0.4131	1773.04919	71.54176	8.0344
2	13.114	MM	0.5358	2.02952e4	631.31335	91.9656

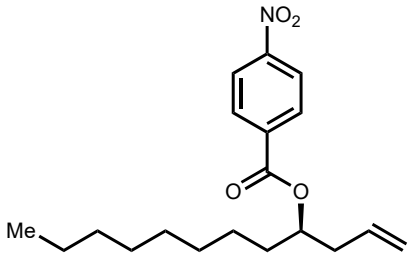

Racemic Sample: Chiralpak OD-H column, 0.05% *i*-PrOH in Hexanes, 120 minutes

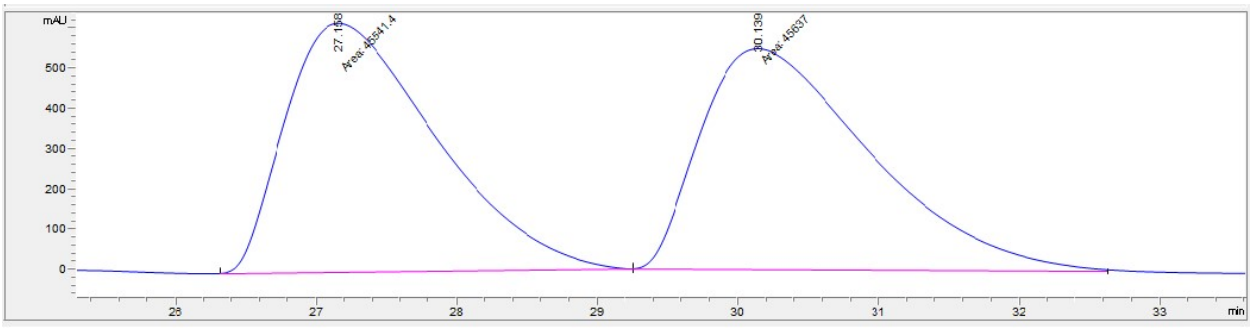

Peak #	RetTime [min]	Type	Width [min]	Area [mAU*s]	Height [mAU]	Area %
1	27.158	MM	1.2338	4.55414e4	615.19806	49.9476
2	30.139	MM	1.3941	4.56370e4	545.58795	50.0524

Scalemic Sample: Chiralpak OD-H column, 0.05% *i*-PrOH in Hexanes, 120 minutes

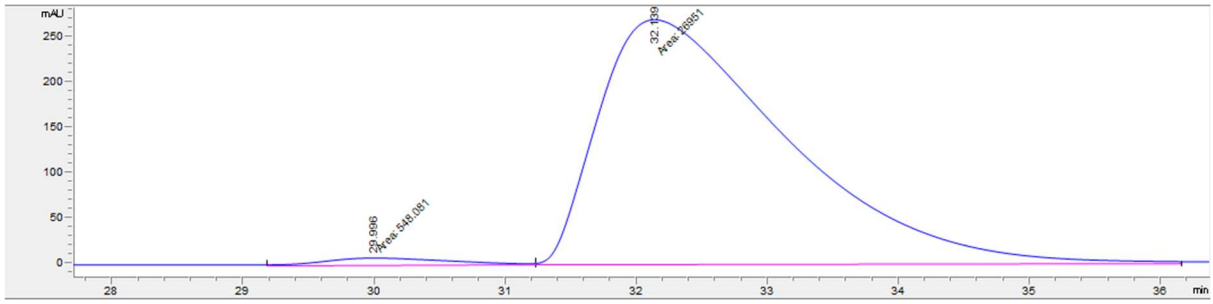

Peak #	RetTime [min]	Type	Width [min]	Area [mAU*s]	Height [mAU]	Area %
1	29.996	MM	1.1188	548.08099	8.16486	1.9931
2	32.139	MM	1.6620	2.69510e4	270.26782	98.0069

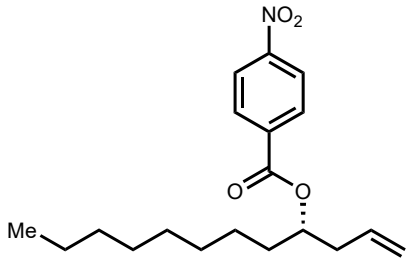

Scalemic Sample: Chiralpak OD-H column, 0.05% *i*-PrOH in Hexanes, 120 minutes

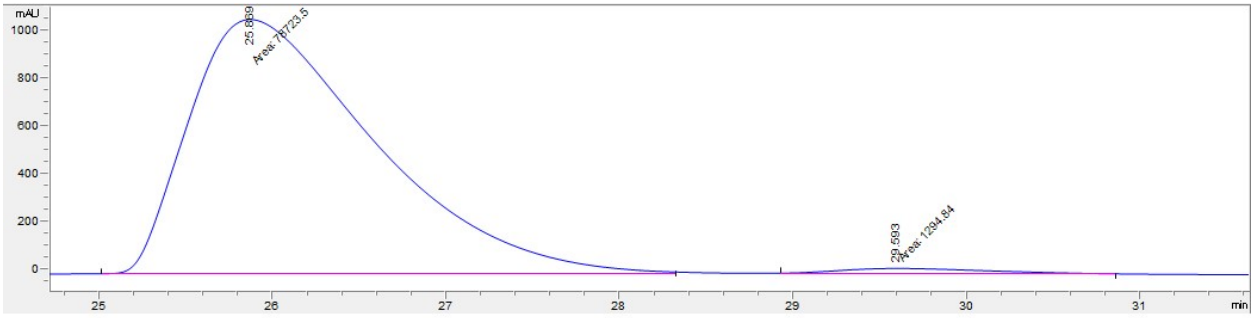

Peak #	RetTime [min]	Type	Width [min]	Area [mAU*s]	Height [mAU]	Area %
1	25.869	MM	1.2326	7.87235e4	1064.48047	98.3818
2	29.593	MM	0.9841	1294.83826	21.92855	1.6182

6. Cell culture and halide quantification from NanoSIMS imaging

Ochromonas danica (CCMP3279 from the National Center for Marine Algae and Microbiota at Bigelow Laboratory) was cultured in YPD medium (10 g yeast extract, 20 g of peptone, and 20 g of glucose in 1 L of water). Cells were grown in 5 mL of YPD in an 8 mL sterile culture tube with a loose cap in a sunny window. We modified the media described by Bruckstein and Scher in order to grow *O. danica* in halide-defined media.[18,19] Cells typically reached stationary phase in 5-20 days under these conditions. For halide-defined media, the following were added to 1 L of water: 0.3 g KH_2PO_4, 1.4 g $MgSO_4•7H_2O$, 0.4 g $MgCO_3$, 0.1 g nitrilotriacetic acid, 0.05 g $CaCO_3$, 1.0 g thiamine mononitrate, 10.0 g glucose, 3.0 g L-glutamate, 0.4 g L-histidine, 0.4 g L-arginine. The pH was adjusted to 5.0 with nitric acid. 1 mL of an essential metal solution consisting of 2 g $Fe(NH_4)_2(SO_4)_2•6H_2O$, 1 g $ZnSO_4•7H_2O$, 0.5 g $MnSO_4•H_2O$, 0.1 g $CoSO_4•7H_2O$, 0.1 g H_3BO_3, 20 mg $CuSO_4•5H_2O$, 50 mg $(NH_4)_6Mo_7O_{24}•4H_2O$, 10 mg Na_3VO_4, 10 mg biotin in 1 L of water was also added to the media. Finally, 0.5 g NH_4Cl, 1.0 g NH_4Br, 1.5 g NH_4I, and 1.3 g NH_4SO_4 were added to separate 1 L portions of media for the chloride-defined, bromide-defined, iodide-defined, and no-halide-added media, respectively. The resulting halide concentration from added halides in each of the halide-defined media was 9.4 mM. The media were sterile filtered, and 10 µL of a suspension of *O. danica* grown in YPD were added to 5 mL aliquots of each medium and left to grow in a sunny window. Cultures were maintained in each of these media by adding a small amount of saturated culture to fresh sterile media when the cultures reached stationary phase.

Cells were fixed with glutaraldehyde and washed with water prior to NanoSIMS analysis in a manner similar to that described for other types of cells.[20] A 1 mL portion of a suspension of cells grown in YPD and each halide-defined medium was added to Eppendorf centrifuge tubes. Cells were gently spun down at 400 g, and the supernatant was removed. The cells were then resuspended in 1 mL of 4% glutaraldehyde (electron microscopy grade from Electron Microscopy Sciences, Hatfield, PA) and fixed for 15 min. The fixed cells were then spun down at 400 g, and the supernatant was removed. The fixed cells were resuspended in 1 mL of water, spun down at 400 g, and the supernatant was again removed. In order to ensure that no salts remained in the cells, they were rinsed twice more with deionized water. After the last centrifugation, the pellet was resuspended in 100 µL of water. 20 µL of each cell suspension was added to a NanoSIMS substrate and allowed to dry overnight in a vacuum desiccator. The substrates were 5 mm x 5 mm pieces diced from a silicon water with a native oxide layer on the surface. The substrates were cleaned in detergent and plasma cleaned immediately before use as described previously.[21] In order to prevent charge buildup during NanoSIMS analysis, we adapted a procedure from the literature for metal coating cells.[22] Substrates with dry cells on the surface were coated with 1.5 nm of a gold/palladium alloy with a Denton Desk sputter coater.

The samples were then introduced into ultra-high vacuum and analyzed with the NanoSIMS 50L at Stanford University. The primary ion beam was a ~2 pA Cs^+ beam focused to an approximately 100 nm diameter spot. The ion detectors were set to $^{12}C^-$, $^{12}C^{14}N^-$, $^{32}S^-$, $^{35}Cl^-$, $^{81}Br^-$, $^{127}I^-$, and $^{197}Au^-$, and secondary electrons were additionally collected. The secondary ion peaks for the halides and Au were

identified with NH_4Cl, NH_4Br, NH_4I, and Au/Pd standards. Cells were imaged in a 20 µm x 20 µm window at 256 px x 256 px for 50 frames. NanoSIMS images were analyzed with ImageJ 4.18 (National Institutes of Health, USA) using the OpenMIMS plugin (Brigham and Women's Hospital Center for NanoImaging, Brigham and Women's Hospital, USA). The first 5 frames were deleted in order to remove contamination from the Au/Pd coating. The remaining 45 frames were summed in OpenMIMS. The halide images were normalized to the $^{12}C^{14}N^-$ image in order to correct for topographical artifacts that change ion yield. Regions of interest were manually drawn over each cell, and the mean halide/$^{12}C^{14}N^-$ ratios within each region were calculated. Note that for Cl and Br, the ratios were adjusted in order to account for the other major stable isotopes (i.e. ^{37}Cl and ^{79}Br). The halide secondary ion intensities were not corrected for their different ionization efficiencies because Cl, Br, and I have similar electron affinities and therefore, negative ionization efficiencies.[23]

In order to quantify the changes in halide abundance among the different growth conditions, the ion counts were summed from a region within the cell body. To correct for differences in ionization efficiency and topography between cells, the total halide counts were normalized to the total $^{12}C^{14}N^-$ counts. Finally, the ratios were corrected to account for the abundances of the stable isotopes of Cl and Br. The final $X^-/^{12}C^{14}N^-$ ratios, shown in Supplementary Table 1, show a dramatic increase in brominated molecules when the cells are grown in medium with bromide as the sole halide source. Notably, there are no detectable iodinated molecules in the cells grown in minimal-iodide medium. Furthermore, as very little iodide is detected in cells from the iodide-defined medium, we are confident that our sample preparation method removed virtually all salts from the cells and that chloride and bromide ions are indeed from halogenated molecules associated with cell membranes.

Halide Quantification From NanoSIMS Imaging

	Rich medium	SD Chloride	SD Bromide	SD Iodide	SD No halide
Cl^-/CN^-	0.201 ± 0.009	0.141 ± 0.009	0.02437 ± 0.00003	0.018 ± 0.003	0.0034 ± 0.002
Br^-/CN^-	0.00006 ± 0.00002	0.00013 ± 0.00007	0.0452 ± 0.0006	0.00010 ± 0.00006	0.00006 ± 0.00004
I^-/CN^-	0.00002 ± 0.00001	0.00003 ± 0.00001	0.00002 ± 0.00001	0.00006 ± 0.00004	0.00004 ± 0.00002
Halide/CN^-	0.201 ± 0.009	0.142 ± 0.009	0.0695 ± 0.0006	0.018 ± 0.003	0.034 ± 0.002

Supplementary Table 1. Halide compositions of cells grown in different media as measured by NanoSIMS. Uncertainties are reported as the standard deviations of different cells. Note that halide/CN^- ratios have not been corrected for the different ion yield of $^{12}C^{14}N^-$ vs. halides. Therefore, the halide ratios can be compared to each other but do not actually provide the ratio of halide to carbon in the samples. Quantities have been corrected for the isotopic abundances of halides.

Thin sections of *O. danica* cells were also imaged with nanoSIMS to investigate the subcellular distribution of chlorosulfolipids. After rinsing the cells with water, the pellet was resuspended in 10% gelatin at 37ºC and centrifuged at 3000g for 5 min. The congealed gelatin was removed from the Eppendorf tube, and the cell pellet at the bottom was removed from the rest of the gelatin. The cell pellet in gelatin was embedded in OCT (optimal cutting temperature) compound as the OCT was freezing over dry ice. The frozen block was cryosection with a cryo-microtome, and the 5 µm sections were placed on 5 mm x 5 mm pieces of silicon wafers. The wafers were rinsed with water to remove OCT and then imaged with nanoSIMS as previously described.

Supplementary Figure 1 shows a representative nanoSIMS ratio image of a section of *O. danica* cells. Green circles identify cells that appear to be sectioned through the middle of the cell. There appears to be chloride, and therefore chlorosulfolipid, enrichment at the edges of the cell and within some intracellular regions of the cell. This data suggests that chlorosulfolipids are primarily localized in the plasma membrane and some organelle membranes, but we cannot identify which organelles from the nanoSIMS images. Future studies could purify organelles from cells and identify chlorosulfolipid enrichment by nanoSIMS imaging or mass spectrometry-based lipidomics.

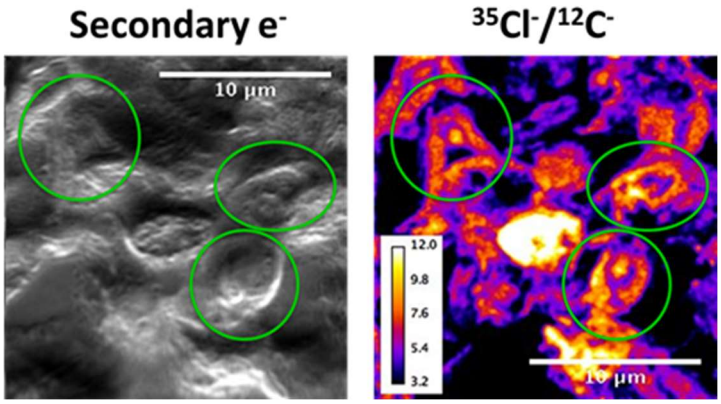

Supplementary Figure 1. NanoSIMS images of thin sections of *O. danica* cells. Green circles identify sectioned cells. Scale bars, 10 µm.

7. Mass spectrometry-based lipidomics

Halosulfolipids were purified from cells according to published protocols.[24] To grow enough cells to isolate halosulfolipids, the 5 mL starter cultures were added to 1 L of each of the halide-defined media. Cells were harvested from 1 L stationary-phase cultures by centrifugation at 15000 g for 30 min. The cell pellets were extracted with 100 mL of 1:1 methanol:ethylacetate. The organic phase was separated and filtered. The halosulfolipid fraction was purified by flash chromatography with 10-30% methanol/dichloromethane. Fractions containing halosulfolipids (as judged by TLC) were pooled and concentrated, yielding a semi-pure green paste. The semi-pure halosulfolipid fractions from cells grown in each medium were then analyzed with LC-MS. Analysis was performed on a Waters Acquity UPLC system equipped with a C8 column and Waters SQD2 with ESI ion source. Halosulfolipid fractions were dissolved in 500 µL methanol, filtered, and 5 µL was injected into the LC-MS instrument. The chromatogram peak corresponding to halosulfolipids was identified via the selected ion chromatogram generated for the danicalipin A **(1)** $[M+H]^-$ ion. Halosulfolipid mass spectra displayed the characteristic isotope distributions. Relative halosulfolipid amounts were estimated by taking the ratio of ion counts of each halosulfolipid species to that of the most abundant species in the mass spectrum.

Supplementary Figure 2 shows the regions of mass spectra containing halosulfolipids for cells grown in each of the different media. The predominant ion in the rich medium is the molecular anion of danicalipin A **(1)**. In the chloride-defined medium, the pentachloride analogue is the most abundant. This medium has a lower chloride concentration than the defined medium. In the bromide-defined medium, the pentabromo analogue is the most abundant, with the fully brominated analogue also being detectable. In the iodide-defined medium, no iodinated analogues are observed, and the tetrachloro analogue is the most abundant. These results indicate that the level of chlorination of danicalipin A is somewhat dependent on the chloride concentration in the medium, but that the deschloro analogue is never the most abundant, suggesting a selection pressure for the halogenation. Finally, consistent with the NanoSIMS data, we directly show that brominated analogues of danicalipin A are synthesized by *O. danica* while iodinated analogues are not.

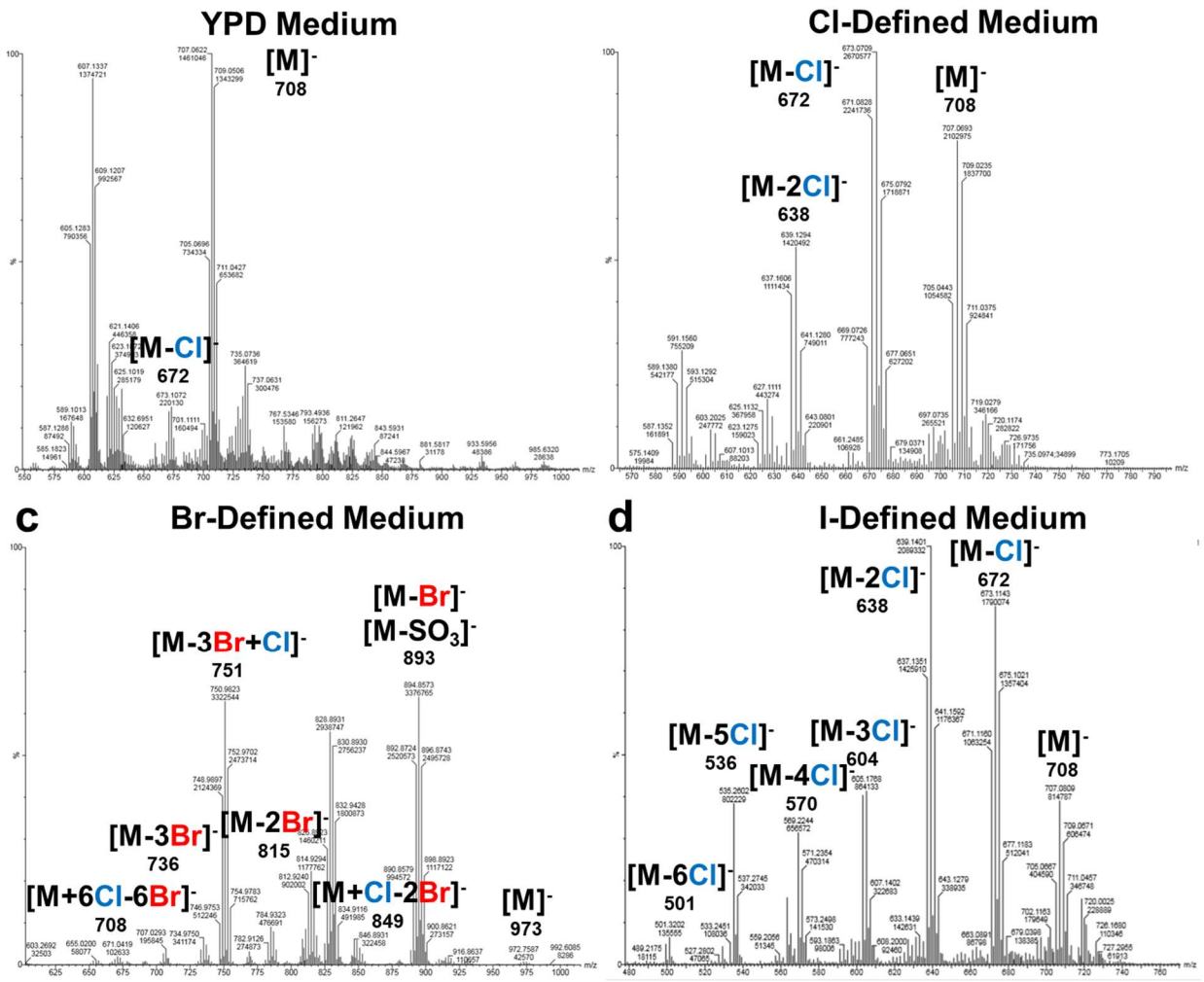

Supplementary Figure 2. Halosulfolipid compositions of cells grown in different media as measured by LC-MS. a) halosulfolipids from cells grown in a rich medium. b) halosulfolipids from cells grown in a Cl-defined medium. c) halosulfolipids from cells grown in a Br-defined medium. d) halosulfolipids from cells grown in an I-defined medium. [M] in (a), (b), and (d) is the molecular ion for danicalipin A **(1)**. [M] for (c) is molecular ion for the fully brominated analogue of danicalipin A. In each of the halide-defined media, the concentration of added halide is 9.4 mM. Chloride concentration in (c) and (d) is from trace contamination. The chloride concentration is (a) > (b) > (c) ≈ (d). The approximate average mass of each species is indicated below its formula.

8. GUV formation and phase behavior of DPTS-sulfolipids GUVs

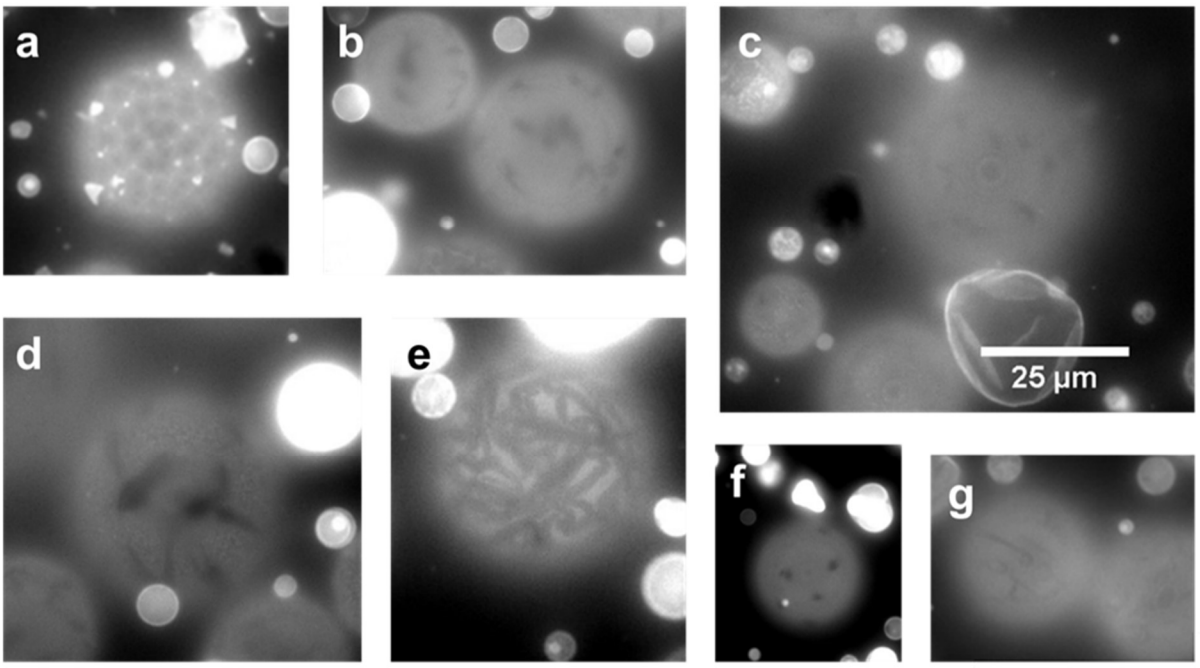

Supplementary Figure 3. Phase separation in DPTS GUVs containing danicalipin A **(1)** and deschlorodanicalipin A **((–)-1B)**. a-g) Domains that exclude TR-DHPE with complex shapes ranging from round to needle-like are observed across a wide variety of DPTS **(3)**:danicalipin A **(1)** ratios. The microscope focal plane was adjusted so that either the top or bottom face of the GUV was in focus.

Giant unilamellar vesicles (GUVs) of mammalian or algal lipids were formed as previously described using the gentle hydration method.[25,26] To form GUVs by gentle hydration, 20 nmol of lipids were mixed in the desired ratios in 2 mL Teflon-capped glass vials. The solvent was evaporated under a gentle stream of argon while rotating the vial. The resulting lipid film was then re-dissolved in chloroform and dried into a film under argon again. Residual solvent was removed by placing the vials in a vacuum desiccator for at least 2 hours. 500 μL of 500 mM sucrose in water was gently added to each vial, and the vial was tightly sealed. The sealed vials were placed in an oven at 60 °C overnight to form GUVs. The vials were then cooled to room temperature, and GUVs were imaged by adding 20 μL of GUV solution to 200 μL of 500 mM glucose in a PDMS well bonded to a glass coverslip. Once the GUVs had sunk, a Nikon Ti-U inverted epifluorescence microscope with a 100X oil immersion objective (Nikon Instruments) equipped with an Andor iXon 897 camera (Andor Technology, Belfast, United Kingdom) was used to image them. Standard emission and excitation filters for Texas Red (ex = 562/40 nm, bs = 593 nm, em = 624/40 nm) were used (Chroma Technology Corp.). The microscope and camera were controlled via Metamorph software (Molecular Devices), and images were processed with ImageJ (National Institutes of Health).

As shown in Supplementary Figure 3, DPTS GUVs containing either danicalipin A **(1)** or deschlorodanicalipin A **((–)-1B)** at a wide range of concentrations displayed phase separation, as

visualized by TR-DHPE fluorescence. The morphologies of these phases ranged from thin needle-like shapes to round. There was no obvious correlation between the concentration or the chlorination of the sulfolipid and the morphology of the domains. TR-DHPE-excluding domains were observed at all sulfolipid concentration where GUVs were formed. The dark domains usually were of smaller surface areas than the surrounding bright phase. As the sulfolipid was the minor component of the GUVs, we assume that the dark domains are enriched in sulfolipid. However, we have no other information about the composition of domains in DPTS/sulfolipid GUVs at this time. On the other hand, no phase separation was observed for GUVs composed of POPC **(2)** and danicalipin A **(1)** (Supplementary Figure 4).

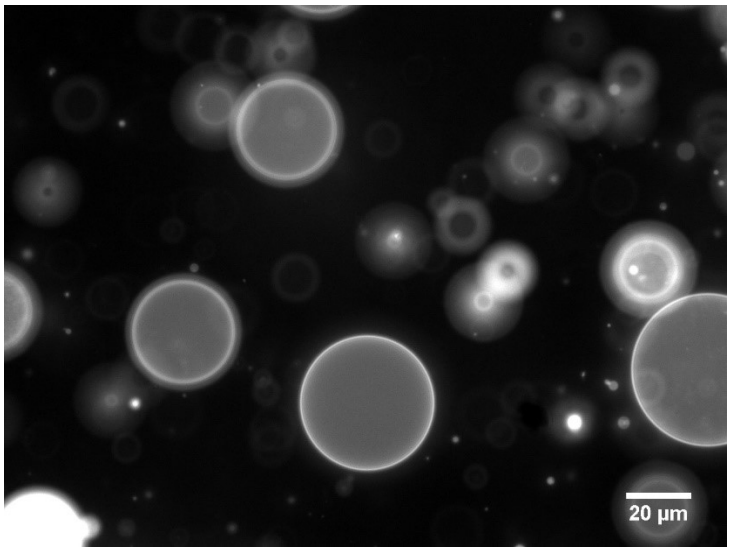

Supplementary Figure 4. GUVs formed from 80:20 POPC **(2)**:danicalipin A **(1)** appear uniform when imaged with TR-DHPE.

9. Cryogenic transmission electron microscopy

SUVs were prepared as described for SAXS analysis. Cryogenic transmission electron microscopy was performed at the Stanford-SLAC CryoEM Facility. 3 µL of a solution of SUVs was applied to a Quantifoil holey carbon grid (Quantifoil Micro Tools GmbH) that was previously glow discharged, blotted for 1-2 seconds, and plunge frozen in liquid ethane using a Leica GP plunge freezer (Leica Microsystems). The frozen grids were imaged with an FEI Tecnai F20 electron microscope (FEI Company) equipped with a Gatan K2 Summit direct detection device (Gatan Inc) with a dose rate of 6-10 e-/px/s. A low pass filter of 0.1 and mean shrink of 4 were applied to the raw images for visualization only. The raw images were processed with RELION 3.0 (Sjors H.W. Scheres, MRC Laboratory of Molecular Biology).[27] Overlapping regions of the bilayers were picked with the manual picking tool, extracted, CTF-corrected, and 2D averaged. The 2D classes with good alignment were reclassified into a single 2D class. The electron scattering profile of the bilayer was calculated by taking a line profile of the 2D classes in ImageJ.[28]

Supplementary Figure 5 shows that at 10 and 30 mol% danicalipin A **(1)** in POPC **(2)**, vesicles remain unilamellar and maintain their gross morphology. Averaging of segments of the bilayers (Supplementary Figure 6) reveals subtle differences between the vesicles with different concentrations of halosulfolipids. Consistent with the SAXS data, cryoEM averages show the bilayer thinning when danicalipin A **(1)** is present (Supplementary Figure 7). We did not collect enough micrographs to quantify the bilayer thicknesses with high precision, but the trend agrees with the higher-precision SAXS data qualitatively.

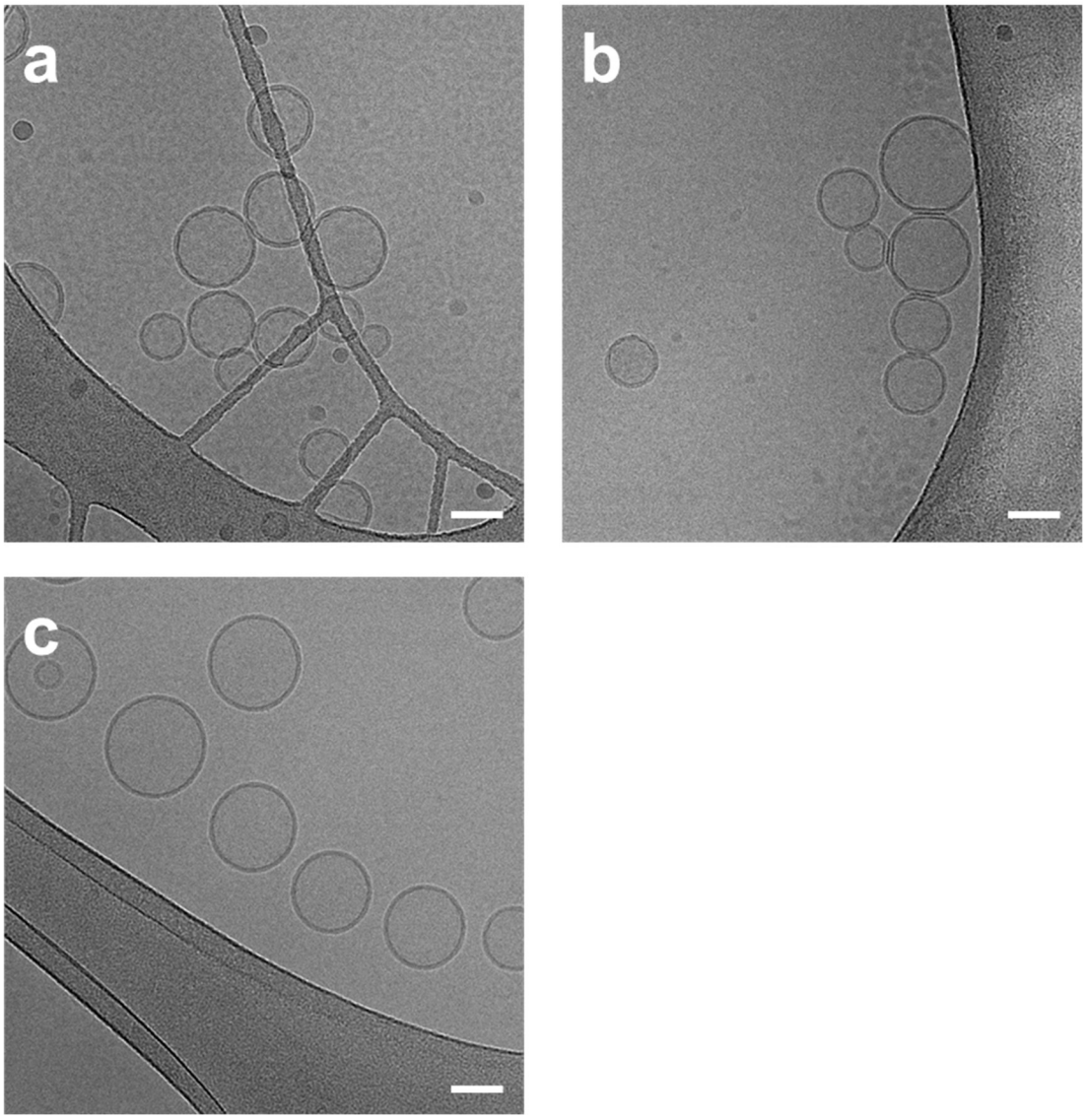

Supplementary Figure 5. Representative micrographs of a) POPC **(2)**, b) POPC **(2)** + 10% danicalipin A **(1)**, and c) POPC **(2)** + 30% danicalipin A **(1)** SUVs in vitreous ice. Scale bars, 50 nm.

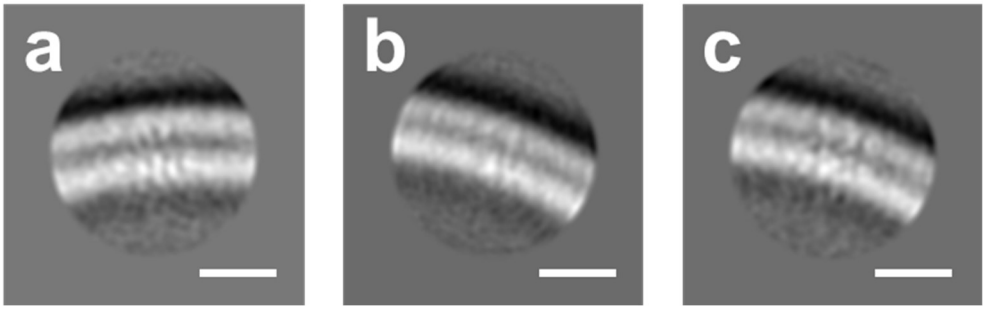

Supplementary Figure 6. 2D class averages of a) POPC **(2)**, b) POPC **(2)** + 10% danicalipin A **(1)**, and c) POPC **(2)** + 30% danicalipin A **(1)** bilayers. Scale bars, 5 nm.

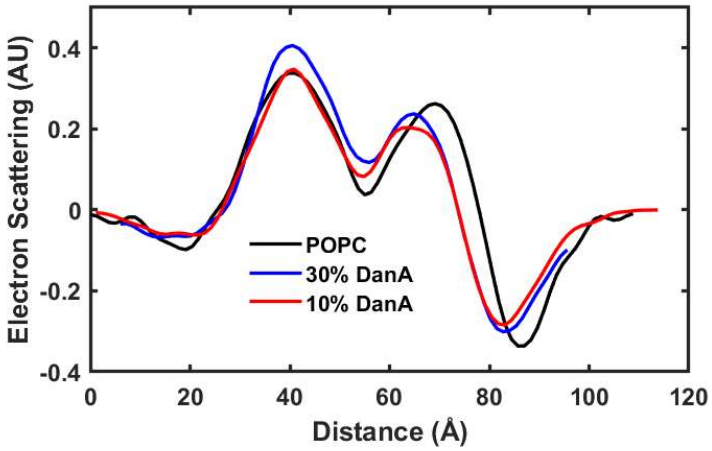

Supplementary Figure 7. Electron scattering profiles from the 2D class averages in Supplementary Figure 6.

10. Pressure-area isotherms of DPPC and cholesterol

Pressure-area isotherms of Langmuir monolayers were recorded using standard techniques with a KSV NIMA KN 2002 (Biolin Scientific) Langmuir trough equipped with a 273 cm^2 Teflon trough and symmetric Delrin barriers.[29] A Wilhelmy plate made of a piece of Whatman #1 filter paper was used to monitor the surface pressure. Water was added to the clean Langmuir-Blodgett trough, and a vacuum line was used to remove any contaminants from the surface before lipid addition. The desired mixtures of lipids and chlorosulfolipids (1 mM in chloroform) were spread onto the surface of the water slowly with a glass microsyringe, and solvent was allowed to evaporate for 10 min. Note that we observed that it was necessary to use chloroform to disperse the lipids at the air-water interface. When methanol was used, much of the lipid was lost to the subphase, generating falsely small mean molecular areas (MMAs). The barriers were then compressed at a rate of 10 mm/min until the isotherm showed that the monolayer had collapsed.

We compared the pressure-area isotherms for monolayers of DPTS **(3)** and halosulfolipds to those of a more conventional lipid mixture, DPPC and cholesterol (Supplementary Figure 8). When cholesterol is included in DPPC monolayers, the MMAs shift to lower values due to the smaller size of cholesterol relative to DPPC. Additionally, the phase transition disappears between 20 and 40 mol% cholesterol. These trends reflect the changes to the phase behavior of the monolayer, as the added cholesterol disorders gel phase DPPC to form a liquid ordered phase. This behavior contrasts with that of DPTS **(3)** and the halosulfolipids analyzed in this work.

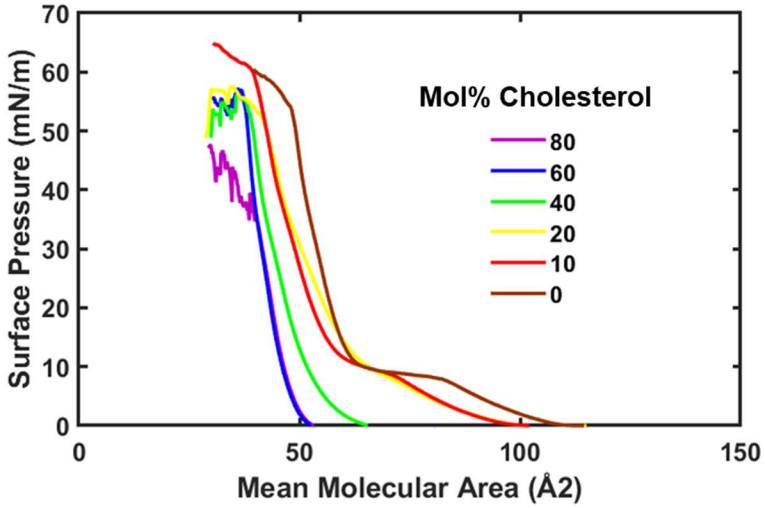

Supplementary Figure 8. Pressure-area isotherms of mixtures of DPPC and cholesterol.

Supplementary Figure 9 shows the monolayer compressibilities calculated from the isotherms in Supplementary Figure 8 at 32 mN/m. The compressibility rises with increasing cholesterol concentrations up to 20 mol% as the cholesterol fluidizes the gel phase DPPC. After the phase transition to the liquid ordered phase, adding more cholesterol rigidifies the monolayer and decreases the compressibility. Again, this behavior stands in contrast to DPTS **(3)** and danicalipin A **(1)**, which continuously increase the

compressibility as its concentration is increases. This suggests that danicalipin A **(1)** disorders and fluidizes gel phase DPTS **(3)** monolayers without causing a first order phase transition.

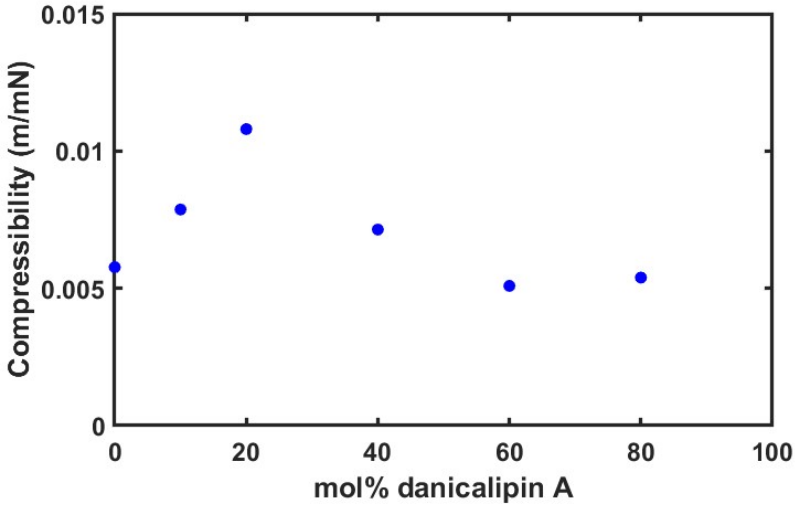

Supplementary Figure 9. Compressibility of mixtures of DPPC and cholesterol.

11. NanoSIMS imaging of POPC SLBs containing danicalipin A

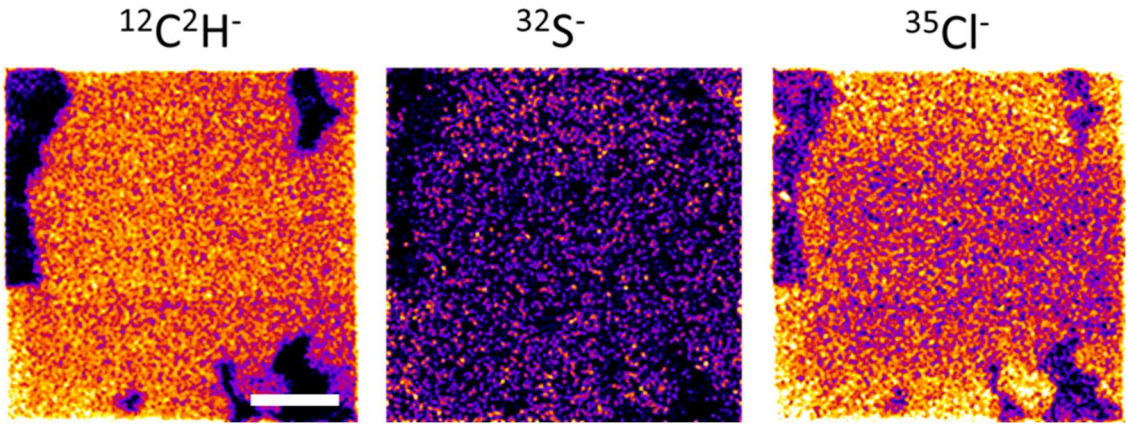

Supplementary Figure 10. SLBs formed from GUVs made with d_{31}-POPC **(2)** + 30 mol% danicalipin A **(1)** contain both sulfur and chloride. Scale bar, 5 μm.

In order to directly show that danicalipin A **(1)** was incorporated into lipid bilayers, we used NanoSIMS to image the atomic composition of supported lipid bilayers formed from a lipid mixture containing danicalipin A **(1)**. GUVs were formed as described in the text from d_{31}-POPC **(2)** + 30 mol% danicalipin A **(1)**. The GUVs were added to plasma cleaned NanoSIMS substrates and allowed to rupture to form isolated SLB patches. After 15 min., the substrates were rinsed with water several times to remove sucrose, salt, and unruptured vesicles. Substrates were flash frozen and freeze dried to remove vitreous ice.[30] SLB patches were then imaged with a 20 μm box and 256 x 256 px. The images were binned 2x to facilitate visualization. The ion images show that in addition to containing ^{2}H from the POPC **(2)**, the SLBs contain both S and Cl, indicating that danicalipin A **(1)** is associated with the bilayers.

12. Small angle X-ray scattering data

SAXS data for small unilamellar vesicles with and without sulfolipids were collected and fit as previously described.[31,32] A thin film of 1 μmol of POPC **(2)** + sulfolipid was hydrated with 250 μL water, vortexed, and then extruded through a 100 nm-pore membrane 31 times. The resulting suspension was then extruded through a 50 nm-pore membrane 31 times to ensure unilamellarity.[33] 30 μL of the resulting suspensions were aliquoted into small centrifuge tubes for SAXS analysis.

Synchrotron SAXS data were collected at beamLine 4-2 of the Stanford Synchrotron Radiation Lightsource (SSRL), Menlo Park, CA.[34] The sample to detector distance was set to 1.1 m and the X-ray wavelength to λ = 1.127 Å (11 keV). Using a Pilatus3 X 1M detector (Dectris Ltd, Switzerland) the setup covered a range of momentum transfer q ≈ 0.017 – 1.17 $Å^{-1}$ where q is the magnitude of the scattering vector defined as $q = 4\pi \sin\theta / \lambda$, with θ the scattering angle and λ the wavelength of the X-rays. Aliquots of 30 μL of freshly extruded vesicles were loaded onto the automated sample loader at the beam line.[35] Consecutive series of sixteen 2 s exposures were collected first from the buffer blank followed by the vesicle samples. Solutions were oscillated in a stationary quartz capillary cell during data collection to maximize the exposed volume in order to reduce the radiation dose per exposed sample volume. The collected data was radially integrated, analyzed for radiation damage, and the buffer was subtracted using the automated data reduction pipeline at the beam line. To improve statistics and check for repeatability the measurements were repeated with different aliquots 8 to 10 times per sample.
The buffer-subtracted and averaged data were fit using the model for unilamellar vesicles,[31] which is based on approximating the electron density of the bilayer by three Gaussian peaks corresponding to the inner and outer phosphate peak and a negative trough at the hydrophobic bilayer center. The following Equation 1 was used for the fits:

$$I(q) = I_0 q^{-2} \sum_{i,j}^{n=3} (R_0 + \varepsilon_i)\left(R_0 + \varepsilon_j\right)\rho_i \rho_j \sigma_i \sigma_j \exp[-q^2(\sigma_i^2 + \sigma_j^2)/2] \cos\left[q\left(\epsilon_i - \epsilon_j\right)\right] + a_0 + a_1 q \quad (1)$$

where R_0 is the mean radius of the vesicle measured at the center of the bilayer, ε is the peak displacements from the bilayer center, σ the Gaussian width of the peak and ρ its amplitude. I_0 is the overall intensity of the measured profile. A background term was added, consisting of a constant a_0 and a linear term a_1, to take into account the contribution from possible lateral correlations. The measured data were fit in the q-region between q = 0.02 – 0.6 $Å^{-1}$. First the data were fit using a simulated annealing routine and the results were then further optimized using a non-linear least square algorithm, both by using code from the open source GNU scientific library project (https://www.gnu.org/software/gsl/).

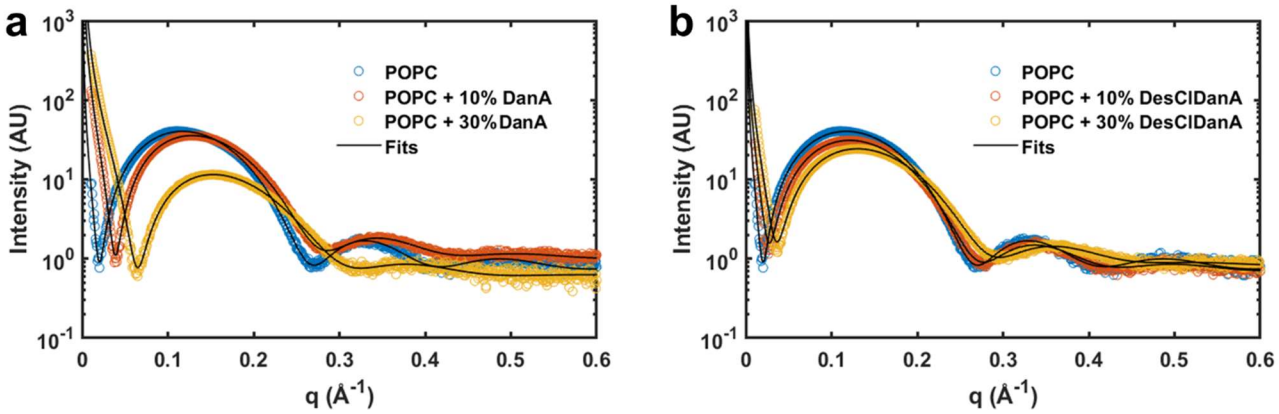

Supplementary Figure 11. Small angle X-ray scattering curves for mixtures of POPC **(2)** and a) danicalipin A **(1)** and b) deschlorodanicalipin A **((–)-1B)**. The fits to the experimental data are shown in black.

Results From Fitting of SAXS Data

Lipid	ρ_1	ε_1	σ_1	ρ_2	σ_2	ρ_3	ε_3
POPC	1.43 ± 0.03	-18.8 ± 0.4	3.53 ± 0.07	-1.00 ± 0.02	6.16 ± 0.12	1.52 ± 0.03	18.4 ± 0.4
POPC + 10% DanA	1.30 ± 0.03	-18.2 ± 0.4	4.28 ± 0.09	-1.00 ± 0.02	6.11 ± 0.12	1.89 ± 0.04	16.8 ± 0.3
POPC + 30% DanA	1.52 ± 0.03	-17.6 ± 0.3	4.03 ± 0.08	-1.00 ± 0.02	5.42 ± 0.11	1.59 ± 0.03	13.2 ± 0.3
POPC + 10% DesCl-DanA	1.32 ± 0.03	-18.4 ± 0.4	3.87 ± 0.08	-1.00 ± 0.02	6.52 ± 0.13	1.55 ± 0.03	17.6 ± 0.3
POPC + 30% DesCl-DanA	1.30 ± 0.02	-16.9 ± 0.3	4.24 ± 0.08	-1.00 ± 0.02	6.93 ± 0.14	1.60 ± 0.03	16.3 ± 0.3

Lipid	σ_3	I_0 [x10^{-7}]	R_0	σ_R	a_0	a_1	χ^2	D = ε_3 - ε_1
POPC	1.66 ± 0.03	16.1 ± 0.3	49.2 ± 1.0	0.22 ± 0.01	0.67 ± 0.01	0.00 ± 0.00	1.76	37.2 ± 0.6
POPC + 10% DanA	1.65 ± 0.03	14.4 ± 0.3	49.9 ± 1.0	0.18 ± 0.003	0.76 ± 0.02	0.22 ± 0.004	0.14	35.0 ± 0.5
POPC + 30% DanA	2.75 ± 0.05	5.48 ± 0.11	50.6 ± 1.0	0.18 ± 0.004	0.50 ± 0.01	0.18 ± 0.004	21.0	30.8 ± 0.4
POPC + 10% DesCl-DanA	1.95 ± 0.04	11.8 ± 0.2	49.9 ± 1.0	0.18 ± 0.004	0.65 ± 0.01	0.00 ± 0.00	0.53	36.0 ± 0.5
POPC + 30% DesCl-DanA	2.16 ± 0.04	10.1 ± 0.2	50.2 ± 1.0	0.18 ± 0.004	0.78 ± 0.02	0.00 ± 0.00	0.29	33.2 ± 0.4

Supplementary Table 2. Parameters from fitting of small angle X-ray scattering data.

13. Comparison of (+)- and (–)-deschlorodanicalipin A

In order to examine the effects of the stereochemistry at the C14 sulfate, we synthesized (+)- and (–)-deschlorodanicalipin A, **(+)-1B** and **(–)-1B**, respectively. We examined the interaction of the two enantiomers with lipid monolayers and lipid bilayers. First, we examined pressure-area isotherms of mixtures of (+)-deschlorodanicalipin A (**(+)-1B**) and DPTS (**3**) as described in the main text for other mixtures of sulfolipids and DPTS. As shown in Supplementary Figure 12a-b, the isotherms for mixtures of **(+)-1B** and **3** are virtually the same as for mixtures of **(–)-1B** and **3**. Both enantiomers show very little binding to monolayers of DPTS **3**, indicating that the chlorination and stereochemistry of chlorines in danicalipin A (**1**) are responsible for membrane interaction. As demonstrated previously for diastereomers of **1**, enantiomers have the same behavior while diastereomers behave differently due to gauche interactions between vicinal chlorines.[36,37]

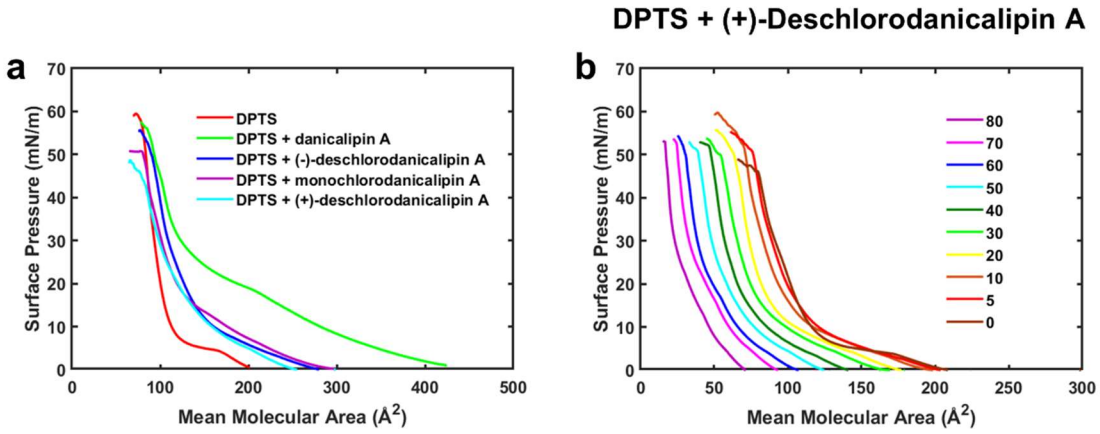

Supplementary Figure 12. Incorporation of danicalipin A (**1**), monochlorodanicalipin A (**1A**), (–)-deschlorodanicalipin A (**(–)-1B**), and (+)-deschlorodanicalipin A (**(+)-1B**) into monolayers of DPTS (**3**). a) Pressure-area isotherms of DPTS (**3**) (red), 1:1 DPTS (**3**):danicalipin A (**1**) (green), 1:1 DPTS (**3**):(–)-deschlorodanicalipin A (**(–)-1B**) (blue), and 1:1 DPTS (**3**):(+)-deschlorodanicalipin A (**(+)-1B**). b) Pressure-area isotherms of mixtures of danicalipin A (**1**) and (+)-deschlorodanicalipin A (**(+)-1B**). DPTS (**3**) makes up the rest of the mol% of the mixture for the indicated sulfolipid mol%.

We also repeated the GUV formation experiments in the presence of (+)-deschlorodanicalipin A (**(+)-1B**), according to the procedure previously described. As with (–)-deschlorodanicalipin A (**1B**), **(+)-1B** induced the formation of fluid GUVs at 10-15 mol% (Supplementary Figure 13). This result indicates that the two enantiomers of deschlorodanicalipin A (**(+)-1B** and **(–)-1B**) interact with lipid bilayers in the same way and that the stereochemistry of the sulfate at C14 is inconsequential in the absence of vicinal chlorines to bias the molecular conformation.

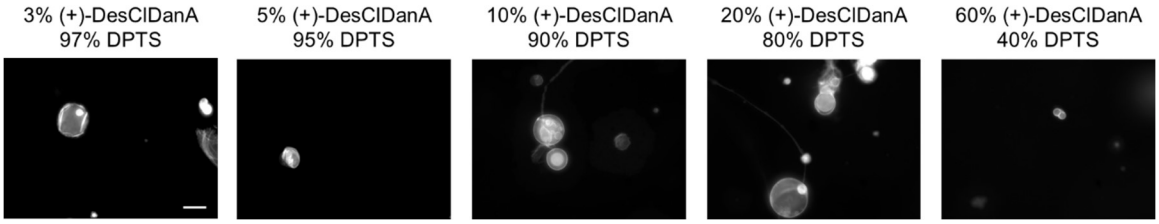

Supplementary Figure 13. Incorporation of (+)-deschlorodanicalipin A (**(+)-1B**) into GUVs of DPTS (**3**) and their influence on DPTS (**3**) phase behavior. (+)-DesClDanA = (+)-deschlorodanicalipin A (**(+)-1B**). Scale bar, 25 μm.

14. References

[1] Halland, N.; Brauton, A.; Bachmann, S.; Marigo, M.; Jørgensen, K. A. (2004) Direct Organocatalytic Asymmetric α-Chlorination of Aldehydes. *J. Am. Chem. Soc*. *126,* 4790-4791.

[2] Kim, I. S.; Ngai, M. Y.; Krische, M. J. (2008) Enantioselective Iridium-Catalyzed Carbonyl Allylation from the Alcohol or Aldehyde Oxidation Level via Transfer Hydrogenative Coupling of Allyl Acetate: Departure from Chirally Modified Allyl Metal Reagents in Carbonyl Addition. *J. Am. Chem. Soc. 130*, 14891-14899.

[3] Fischer, S.; Huwyler, N.; Wolfrum, S.; Carreira, E. M. (2016) Synthesis and Biological Evaluation of Bromo- and Fluorodanicalipin A. *Angew. Chem. Int. Ed. 55*, 2555-2558.

[4]Tonoi, T.; Kawahara, R.; Inohana, T.; Shiina, I. (2016) Enantioselective total synthesis of naturally occurring eushearilide and evaluation of its antifungal activity. *J Antibiot. 69*, 697–701.

[5] Halland, N.; Brauton, A.; Bachmann, S.; Marigo, M.; Jørgensen, K. A. (2004) Direct Organocatalytic Asymmetric α-Chlorination of Aldehydes. *J. Am. Chem. Soc. 126*, 4790-4791.

[6] Kawahara, T.; Kumaki, Y.; Kamada, T.; Ishii, T.; Okino, T. (2009) Absolute Configuration of Chlorosulfolipids from the Chyrsophyta *Ochromonas* danica. J*. Org. Chem*. *74*, 6016–6024

[7] Kumaraswamy, G.; Sadaiah, K.; Raghu, N. (2012) An organocatalytic enantioselective synthesis of (+)-duryne. *Tetrahedron: Asymmetry*, *23*, 587-593.

[8] Bailey, A. M.; Wolfrum, S.; Carreira, E. M. (2015) Biological Investigations of (+)-Danicalipin A Enabled Through Synthesis. *Angew. Chem. Int. Ed. 55*, 639-643.

[9] Landry, M. L.; Hu, D. X.; McKenna, G. M.; Burns, N. Z. (2016) Catalytic Enantioselective Dihalogenation and the Selective Synthesis of (-)-Deschloromytilipin A and (-)-Danicalipin A. *J. Am. Chem. Soc*. *138*, 5150-5158.

[10] Woerly, E. M.; Struble, J. R.; Palyam, N.; O'Hara, S. P.; Burke, M. D. (2011) (1-bromovinyl)-MIDA boronate: a readily accessible and highly versatile building block for small molecule synthesis. *Tetrahedron 67*, 4333−4343.

[11] Hoffman, R. W.; Ditrich, K.; Köster, G.; Stürmer, R. (1989) Stereoselective synthesis of alcohols, XXXI: Stereoselective C-C bond formation using chiral Z-pentenylboronates. *Chem. Ber. 122*, 1783−1789.

[12] Matteson, D. S.; Majumdar, D. (1980) Directed chiral synthesis with pinanediol boronic esters. *J. Am. Chem. Soc*. *102*, 7588−7590.

[13] Matteson, D. S. (2013) Boronic Esters in Asymmetric Synthesis. *J. Org. Chem. 78*, 10009−10023.

[14] Chen, J. L.-Y.; Scott, H. K.; Hesse, M. J.; Willis, C. L.; Aggarwal, V. K. Highly Diastereo- and Enantioselective Allylboration of Aldehydes using alpha-Substituted Allyl/Crotyl Pinacol Boronic Esters via in Situ Generated Borinic Esters. *J. Am. Chem. Soc*. **2013**, *135*, 5316−5319.

[15] Chen, J. L.-Y.; Scott, H. K.; Hesse, M. J.; Willis, C. L.; Aggarwal, V. K. (2014) Highly Diastereoselective and Enantiospecific Allylation of Ketones and Imines Using Borinic Esters: Contiguous Quaternary Stereogenic Centers. *Angew. Chem., Int. Ed*. *53*, 10992−10996.

[16] Negoro, T.; Ikeda, Y. (1984) Bromochlorination of alkenes with dichlorobromate(1-) ion. II. Regio- and stereochemistry for the bromochlorination of 1-phenylpropenes with dichlorobromate(1-) ion. *Bull. Chem. Soc. Jpn*. *57*, 2111− 2115.

[17] Popov, A. I.; Buckles, R. E. (1957) Polyhalogen Complex Salts. *Inorg. Synth*. *5*, 167−175.

[18] Aaronson, S.; Scher, S. (1960) Effect of Aminotriazole and Streptomycin on Multiplication and Pigment Production of Photosynthetic Microorganisms. *J. Eukaryot. Microbiol*. *7*, 156-158.

[19] Bruckstein, A. H. (1970) Can an Organism Bio-Synthesize a Bromosulfolipid? *Baskerville Chem. J. 18*, 3−4.

[20] Nuñez, J.; Renslow, R.; Cliff III, J. B.; Anderton, C. R. (2017) NanoSIMS for biological applications: Current practices and analyses. *Biointerphases 13*, 03B301.

[21] Rawle, R. J.; Boxer, S. G.; Kasson, P. M. (2016) Disentangling Viral Membrane Fusion from Receptor Binding Using Synthetic DNA-Lipid Conjugates. *Biophys. J*. *111*, 123-131.

[22] Frisz, J. F.; Lou, K.; Klitzing, H. A.; Hanafin, W. P.; Lizunov, V.; Wilson, R. L.; Carpenter, K. J.; Kim, R.; Hutcheon, I. D.; Zimmerberg, J.; Weber, P. K.; Kraft, M. L. (2013) Direct chemical evidence for sphingolipid domains in the plasma membranes of fibroblasts. *Proc. Natl. Acad. Sci. U.S.A*. *110*, 613-622.

[23] Wilson, R. G.; Novak, S. W. (1991) Systematics of secondary-ion-mass spectrometry relative sensitivity factors versus electron affinity and ionization potential for a variety of matrices determined from implanted standards of more than 70 elements. *J. Appl. Phys*. *69*, 466-474.

[24] White, A. R.; Duggan, B. M.; Tsai, S. C.; Vanderwal, C. D. (2016) The Alga Ochromonas danica Produces Bromosulfolipids. *Org. Lett*. *18*, 1124-1127.

[25] Reeves, J. P.; Dowben, R. M. (1969) Formation and properties of thin-walled phospholipid vesicles. *J. Cell. Physiol*. *73*, 49–60.

[26] Walde, P.; Cosentino, K.; Engel, H.; Stano, P. (2010) Giant vesicles: preparations and applications. *ChemBioChem 11*, 848-865.

[27] Zivanov, J.; et al. (2018) New tools for automated high-resolution cryo-EM structure determination in RELION-3. *Elife 7*, e42166.

[28] Schindelin, J.; et al. (2012) Fiji: an open-source platform for biological-image analysis. *Nat. Methods 9*, 676-682

[29] Girard-Egrot, A. P.; Loïc J. (2007) Langmuir-Blodgett Technique for Synthesis of Biomimetic Lipid Membranes. In *Nanobiotechnology of Biomimetic Membranes* (Martin, D. K., Ed.) Springer: New York.

[30] Moss, F. R.; Boxer, S. G. (2016) Atomic Recombination in Dynamic Secondary Ion Mass Spectrometry Probes Distance in Lipid Assemblies: A Nanometer Chemical Ruler. *J. Am. Chem. Soc*. *138*, 16737-16744.

[31] Brzustowicz, M. R.; Brunger, A. T. (2005) X-ray scattering from unilamellar lipid vesicles. *J. App. Cryst. 38*, 126-131.

[32] Moss III, F. R.; Shuken, S. R.; Mercer, J. A. M.; Cohen, C. M.; Weiss, T. M.; Boxer, S. G.; Burns, N. Z. (2018) Ladderane phospholipids form a densely packed membrane with normal hydrazine and anomalously low proton/hydroxide permeability. *Proc. Natl. Acad. Sci. U.S.A*. *115*, 9098-9103.

[33] MacDonald, R. C.; MacDonald, R. I.; Menco, B. P.; Takeshita, K.; Subbarao, N. K.; Hu, L. R. (1991) Small-volume extrusion apparatus for preparation of large, unilamellar vesicles. *Biochim. Biophys. Acta*. *1061*, 297-303.

[34] Smolsky, I. L.; Liu, P.; Niebuhr, M.; Ito, K.; Weiss, T. M.; Tsuruta, H. (2007) Biological small-angle X-ray scattering facility at the Stanford Synchrotron Radiation Laboratory. *J. App. Cryst. 40*, S453-S458.

[35] Martel, A.; Liu, P.; Weiss, T. M.; Niebuhr, M.; Tsuruta, H. (2012) An integrated high-throughput data acquisition system for biological solution X-ray scattering studies. *J. Synchrotron Radiat. 19*, 431-434.

[36] Boshkow, J.; Fischer, S.; Bailey, A. M.; Wolfrum, S.; Carreira, E. M. (2017) Stereochemistry and biological activity of chlorinated lipids: a study of danicalipin A and selected diastereomers. *Chem. Sci*. *8*, 6904-6910.

[37] Umezawa, T.; Shibata, M.; Kaneko, K.; Okino, T.; Matsuda, F. (2011) Asymmetric total synthesis of danicalipin A and evaluation of biological activity. *Org. Lett*. *13*, 904-907.